Targeting Epsins to Inhibit FGF Signaling while Potentiating TGF-β Signaling Constrains Endothelial-to-Mesenchymal-Transition in Atherosclerosis

Yunzhou Dong, Ph.D.[1,2]*†, Beibei Wang, M.D., Ph.D.[1,2]†, Mulong Du, M.D., Ph.D.[3]†, Bo Zhu, M.D., Ph.D.[1,2], Kui Cui, Ph.D.[1,2], Kelvin Chan, Ph.D.[1,2], Douglas B. Cowan, Ph.D.[1,2], Sudarshan Bhattacharjee, Ph.D.[1,2], Scott Wong, B.S.[1], Joyce Bischoff, Ph.D.1,2, MacRae F. Linton, M.D., Ph.D.[4], and Hong Chen, Ph.D.[1,2]*

1. Vascular Biology Program, Boston Children's Hospital, Boston, MA 02115
2. Department of Surgery, Harvard Medical School, Boston, MA 02115
3. Department of Environmental Health, Harvard T.H. Chan School of Public Health, Boston, MA 02115
4. Department of Medicine, Vanderbilt University Medical Center, Nashville, TN 37232

Running title: Epsins Potentiate EndoMT in Atherosclerosis

* Correspondence to Hong Chen and Yunzhou Dong
Vascular Biology Program, Karp Family Research Laboratories, Boston Children's Hospital, Harvard Medical School, 1 Blackfan Circle, Boston, MA 02115
Tel: 617-919-6304; Fax: 617-730-0232
hong.chen@childrens.harvard.edu and yunzhou.dong@childrens.harvard.edu

† Y Dong, B Wang, and M Du contributed equally to this work.

ABSTRACT

BACKGROUND: Epsin endocytic adaptor proteins are implicated in the progression of atherosclerosis; however, the underlying molecular mechanisms have not yet been fully defined. In this study, we determined how epsins enhance endothelial-to-mesenchymal transition (EndoMT) in atherosclerosis and assessed the efficacy of a therapeutic peptide in a preclinical model of this disease.

METHODS: Using single cell RNA sequencing (scRNA-seq), combined with molecular, cellular, and biochemical analyses, we investigated the role of epsins in stimulating EndoMT using knock-out mouse models. The therapeutic efficacy of a synthetic peptide targeting atherosclerotic plaques was then assessed in *Apoe*$^{-/-}$ mice.

RESULTS: ScRNA-seq and lineage tracing revealed that epsins 1 and 2 promote EndoMT, and the loss of endothelial epsins inhibits EndoMT marker expression as well as transforming growth factor-beta signaling *in vitro* and in atherosclerotic mice, which is associated with smaller lesions in *Apoe*$^{-/-}$ mouse model. Mechanistically, the loss of endothelial cell epsins results in increased fibroblast growth factor receptor-1 (FGFR1) expression that inhibits TGF-β signaling and EndoMT. Epsins directly bind ubiquitinated FGFR1 through their ubiquitin-interacting motif (UIM), which results in endocytosis and degradation of this receptor complex. Consequently, administration of a synthetic UIM–containing peptide API significantly attenuates EndoMT and progression of atherosclerosis.

CONCLUSIONS: We conclude that epsins potentiate EndoMT during atherogenesis by increasing TGF-β signaling through FGFR1 internalization and degradation. Inhibition of EndoMT by reducing epsin-FGFR1 interaction with a therapeutic peptide may represent a novel treatment strategy for atherosclerosis.

Key Words: Epsin, adaptor protein, endocytosis, endothelial-to-mesenchymal transition (EndoMT), TGF-ß signaling, FGFR1, atherosclerosis, single cell RNA sequencing, vascular disease, peptide therapy

INTRODUCTION

Atherosclerosis is one of the most challenging vascular diseases to cure, and it has been causally linked with heart attacks and strokes. Generally, the disease involves multiple cell types, including endothelial cells, vascular smooth muscle cells, immune cells, and others[1]. One of the major pathological features of atherosclerosis is the accumulation of arterial plaques that can progress from simple fatty streaks to complex lesions that can reduce blood flow or rupture leading to thrombosis and ischemic cardiovascular events [1, 2]. At the tissue level, each cell type can contribute to atherosclerosis; however, the endothelium has been proposed to be crucial for the initiation and progression of atherosclerosis[3, 4].

Chronic vascular inflammation is a hallmark of atherosclerosis[5] and induces endothelial-to-mesenchymal transition (EndoMT)[6]. During EndoMT, vascular smooth muscle cell (VSMC) or mesenchymal stem cell-like markers, such as α-SMA, SM22α, Collagen 1a, Fibronectin, and N-cadherin, are expressed in endothelial cells[7, 8]. This process is thought to allow mesenchymal transition of non-SMC-derived cells that are capable of maintaining indices of lesion stability; however, this temporary protection is lost when atherosclerosis progresses to a more advanced stage, presumably because of increased inflammation associated with the advanced lesion[9]. Furthermore, other studies suggest that EndoMT exacerbates vascular inflammation in atherosclerosis[10, 11].

It is known that TGF-ß signaling is a primary driver of EndoMT[12, 13], while disturbed shear stress and cytokines are the most common activating modulators for TGF-ß signaling[11]. In contrast, FGFR1 signaling has been proposed as an endogenous inhibitor that suppresses the TGF-ß pathway[7, 11]. Using an endothelial lineage tracing approach supported by cell-specific marker staining[10, 14], EndoMT has been linked to multiple cardiovascular[15-17] and metabolic diseases, including atherosclerosis, obesity, hypertension, hyperlipidemia, and diabetes[7]. As a result, EndoMT has been suggested to be a target for treating vascular diseases[11, 18-20], including atherosclerosis.

Epsins are ubiquitously-expressed adaptor proteins involved in the regulation of the endocytosis[21, 22] of plasma membrane receptors complexes[23-27], which facilitates their degradation to influence endothelial cell signaling[23, 25-27]. Using epsin mutant mouse models, we have discovered that these proteins regulate Notch, VEGFR2, and VEGFR3[23-28] by binding to ubiquitinated membrane receptors to physiologically or pathologically modulate cell function in embryogenesis[28], angiogenesis, lymph angiogenesis[23, 25-27]. Our previous reports showed epsins promote atherosclerosis in the endothelium and in macrophages.

Deletion of epsins in endothelial cells attenuates atherosclerosis by stabilizing IP3R1 degradation[29] and by blunting inflammatory signaling through TLR2/4[30] in the *Apoe*$^{-/-}$ atherosclerosis mouse model, suggesting that epsins promote atherosclerosis by modulating inflammatory signaling pathways. Macrophage-deficient epsins also reduce atherosclerosis by binding to the LDL Receptor-related Protein 1 (LRP-1) to increase efferocytosis[31]. Loss of epsins in macrophages decreases pro-inflammatory M1 macrophages and increases anti-inflammatory M2 macrophages[31]. These observations suggest that epsins promote atherosclerosis by regulating inflammation.

To investigate the role of epsins in EndoMT, we generated inducible mutant mice lacking epsins 1 and 2 in endothelial cells and bred these mice into an atherosclerotic (*i.e.,* *Apoe*$^{-/-}$) background[29]. Here, we show that epsins are required for EndoMT, and that the loss of these proteins in the endothelium reduces EndoMT by permitting sustained FGFR1 signaling by inhibiting the degradation of this receptor complex. Importantly, we demonstrate the efficacy of blocking epsin-FGFR1 interactions specifically in atheromas using systemic administration of a targeted epsin UIM-containing peptide to inhibit EndoMT and atherosclerosis progression; thereby, providing a new approach to combat this disease.

METHODS

ScRNA-seq datasets have been deposited in a publicly available repository as indicated below. All other data that support the findings of this study are available from the corresponding authors on reasonable request.

Genetic mouse models

Mice used in this study are C57Bl6/J genetic background. C57Bl6/J strain is defined as wild type (WT). EC-specific deletion of epsin was established by crossing Epsin $1^{fl/fl}$: Epsin $2^{-/-}$ mice with endothelial cell (EC)-specific Cre transgenic iCDH5-Cre mice, and these mice were bred with the *Apoe*$^{-/-}$ atherosclerotic mouse model and backcrossed seven times. Mice with an inducible deletion of endothelial Epsins 1 and 2 on an *Apoe*$^{-/-}$ background (EC-iDKO/*Apoe*$^{-/-}$) were fed a Western Diet (WD) for 12 to 14 weeks beginning at 8 weeks of age[32, 33]. Aortic roots and hearts were isolated and processed for evaluation of atherosclerotic lesion as previously described[29, 31-33]. Lesion area was quantified using NIH Image J.

Evaluation of EndoMT markers by immunostaining *in vivo* and *in vitro*

Apoe$^{-/-}$ mice, EC-iDKO/*Apoe*$^{-/-}$, control, or API peptide-treated mice were evaluated by co-staining CD31 with EndoMT markers, including αSMA, MyH11, SM22, and Calponin. EndoMT is expressed by the overlapping percentile (%) of CD31 with VSMC markers. For *in vitro* EndoMT marker staining, mouse aortic endothelial cell (MAEC) cultures were treated with TGFβ (10 ng/mL) as indicated.

Aortic sample preparation for single cell RNA sequencing (scRNA-seq)

Mouse aortas were cut into fine pieces and placed in 6.5 mL enzyme solution at 37°C for 1.5 hours (5 mL DMEM, 1 mL trypsin, collagenase type I 10 mg/mL, collagenase type IV 10 mg/mL , 50 µL elastin (2.5 mg/mL stock), collagenase type II 200 µL (stock: 1 mg/mL), Collagenase XI 200 µL (stock: 1 mg/mL), Hydrolase 200 µL (stock: 1 mg/mL), Liberase 100 µL (stock: 3.85 mg/mL, Roche), DNase I 10 µL (stock: 5U/µL, Sigma). This solution was then filtered using a 40 µm strainer (Falcon, NC), centrifuged (400xg for 5 min) and the cell pellet was suspended in 90 µL FEB buffer containing 0.5% BSA and 2 mM EDTA

in PBS. 10 μL of CD31 Microbeads (MACS) was added to the suspension at 4°C for 15 min. Microbeads were passed through a LS column (MACS), Cells were processed for scRNA-seq using the 10xGenomics platform and sequencing was performed by BGI-HK.

Data analysis of single cell RNA seq

We used the Cell Ranger and R package Seurat v.4.0.2[34] to perform scRNA-seq analysis. Briefly, we generated a normalized gene expression matrix harboring a total of 5,016 and 5,521 cells for EC-iDKO and WT mouse models, respectively, which were then integrated using multiple canonical correlation analysis (CCA). Two-dimensional Uniform Manifold Approximation and Projection (UMAP) and Graph-based clustering were used for visualization. To validate our results, we empirically introduced well-defined markers, including Pecam1, Cdh5, Cldn5, Tek, and Notch1 for EC cells and Acta2, Tagln, Cald1, Mylk, and Col1a1 for VSMC cells, to explore cell types from cell clusters. Differential gene expression between groups of interest was performed using FindMarkers function implemented in Seurat. Genes with log2 fold change > 0.5 and $P < 0.05$ were considered differentially expressed. Pathway enrichment analysis for group comparison was performed via R package ReactomeGSA (https://github.com/reactome/ReactomeGSA) using the 'analyze_sc_clusters' function. The trajectory inference for single cell data from EndoMT models was performed via R package slingshot [PMID: 29914354][35].

Lineage tracing

TdTomato mice were bred to WT or EC-iDKO mice to create WT: TdTomato and EC-iDKO: TdTomato mice, and these mice were then bred to iCDH-cre mice to establish WT: TdTomato: iCDH-cre and EC-iDKO: TdTomato: iCDH-cre mice. Tamoxifen was given to these mice seven times to delete epsins and activate the expression of the TdTomato gene. At 8 weeks of age, these mice were fed a WD for 8 weeks. Aortic roots and arches were fixed and immunostaining with CD31 prior to image acquisition using a confocal microscope (LSM880, Carl Zeiss).

Administration of synthetic peptides (Control and API) to *Apoe*$^{-/-}$ mouse model

(1) Prevention protocol: Eight-week-old male *Apoe*$^{-/-}$ mice were fed a WD for eight weeks and injected with Control or API peptides. The dose of each peptide was 25 mg/kg, with two injections per week, I.V. for two months.
(2) Therapeutic protocol: Eight week old male *Apoe*$^{-/-}$ mice were fed a WD for 6 weeks, and split into two groups: control or API peptides. Peptides were administered as described above for 6 weeks. The dose of each peptide was 25 mg/kg, with two injections per week, I.V. injection.

Cell migration assay

A Boyden chamber assay protocol was used in this study to assess cell migration as modified from Wang et al[36]. In brief, we isolated MAECs from WT and EC-iDKO mouse aortas as previously described[29]. Cells were treated by 5 μM tamoxifen for 4 days to delete epsins, followed by the 10 ng/mL TGF-ß treatment for another 4 days. Cells were trypsinized and counted by microscopy. 750 μL test medium with or without 10% FBS was added in the 24-well plate wells, and 50K cells in 500 μL DMEM were added into the upper chamber. The plate was kept in the 37°C CO_2 incubator for 7 hours. The non-migrated cells on the upper side of the membrane were removed using a cotton swab. Cells were then fixed by methanol and stained by eosin[36]. Images were captured using inverted microscopy (Axio Observer, Zeiss).

Cell surface FGFR1 biotinylation and western blot analysis

FGFR1 biotinylation was performed as described previously for VEGFR2[25]. Biotinylated surface FGFR1 was detected by western blotting using an anti-FGFR1 antibody and transferrin served as internal control.

Standard methods

Isolation of primary mouse aortic endothelial cells (MAECs) and generation of epsin-deficient cells (DKO) *in vitro* were performed as previous report[29]. Western blotting, Immunoprecipitation (IP) analysis, immunostaining, and cell culture were performed according to routine methodologies in our laboratory[23, 25]. Plasmids or siRNA transfection, electroporation, and RT-PCR were performed as described[23, 25, 27].

Study approval

Animal studies were approved by the Institutional Animal Care and Use Committee (IACUC) at Boston Children's Hospital.

Statistical analysis

Statistical analysis was conducted using Prism 8.0 (GraphPad Software). Data are presented as mean ± SEM. Data were analyzed by two-tailed, unpaired or paired Student's *t*-test or ANOVA A *p* value of less than 0.05 was considered statistically significant.

RESULTS

Single cell RNA sequencing revealed epsins play a critical role in EndoMT

To investigate whether epsins play a role in EndMT, we performed scRNAseq analysis. WT and EC-iDKO mice were fed western diet (WD) for 14 weeks, followed by the isolation of aortas and enzymatic digestion (Supplemental Figure 2; Supplemental Methods) and scRNA seq. Our data show that the two groups of cells from WT and EC-iDKO were well distributed and merged using Principal Component Analysis (PCA) and Uniform Manifold Approximation and Projection for Dimension Reduction (UMAP) plot (Figure 1A & B). We then divided the cell population into 10 clusters. Again, the UMAP distribution in WT and EC-iDKO group are similar, comparable and nonbiased (Figure 1C). Together, all these data suggest our data quality control is appropriate.

We then analyzed established markers of endothelial and VSMC, and we found that five EC markers Pecam1, Cdh5, Cldn5, Tek and Notch1 were all exclusively expressed in cluster 4 in the EC-iDKO population. The same was observed in WT mice, except Pecam1, which was also expressed in group 5-10 (possibly immune cells) (Supplemental Figure 3); this data strongly suggests that cluster 4 is the EC enriched population. The SMC specific marker genes are all expressed in 1-10 groups in EC-iDKO and WT population with different expression levels (Supplemental Figure 3).

Since clusters 1-3 do not express any EC marker genes but only express SMC marker genes, these three groups are defined as SMC or SMC-like cell population (Supplemental Figure 3). We then use Pecam1 and collagen a1 (Col1a1) to pinpoint EC and SMC marker population in UMAP (Figure 1D), and it is obvious that these two clusters have overlapping cells that co-express endothelial and SMC markers; we defined this group of cells as P^+/C^+ cells. The proportion of Pecam1 and Col1a1 is plotted in Figure 2E (p=8.08e-13). For the Pecam1 positive cluster, we further divided it into 4 groups by Pecam1 and collagen 1a1 (Col1a1, SMC marker) as displayed in Figure 1E, in which $Pecam1^+/Col1a1^-$ population or endothelial cells is 1.45 fold in EC-iDKO versus WT, a 45% increase in EC-iDKO mice; while the P^+/C^+ cells in WT is 2.7 fold increase compared

to EC-iDKO, suggesting that more ECs are becoming P^+/C^+ cells in WT, while loss of epsins in endothelium significantly blocked the process of EC transforming towards SMC.

This result is supported by measuring specific EC and SMC markers in Pecam1+ cluster. As shown in Figure 1F & 1G, violin plots show that EC markers (Pecam1, Cdh5, Cldn5, Tek and Notch1) are significantly upregulated in EC-iDKO aortas than that in WT aortas, while SMC markers are downregulated in EC-iDKO mice; importantly, Col1a1 is exclusively expressed in WT but seldom expressed in EC-iDKO mice. Together, loss of epsins from the endothelium significantly blocks the EndMT.

Trajectory of EC to SMC differentiation in WT and EC-iDKO mice subjected to inflammatory stimuli

As displayed in Figure 1H & I, as well as Supplemental Figure 4H, the trajectory plot clearly demonstrated the transition of EC to P^+/C^+ and SMC process by EC marker Pecam1 and SMC marker Tagln in WT and EC-iDKO cell population. Similarly, all the tested EC and SMC markers showed the similar tendency by using integrated population of WT and EC-iDKO cells, (Supplemental Figure 4B & C).

To mimic the EndMT with the “time” change, we plotted EC, P^+/C^+ cells and SMC in PCA plot, and performed pseudotime analysis. As suggested by Figure 1J & K, the three populations clearly clustering, overlapping and showed a typical different cell type distribution in pseudotime axis, suggesting EC→ P^+/C^+ →SMC cell type transition.

TdTomato lineage tracing shows epsins are crucial to promote EndoMT

We demonstrated that oxLDL stimuli and WD-fed *Apoe*$^{-/-}$ mice upregulate epsin expression in endothelium in our previous report[29]. EndoMT has been positively linked in human atherosclerosis[7]. These results imply that epsins are associated with EndoMT in atherosclerosis. To further test our hypothesis, we bred the transgenic TdTomato mice to EC-iDKO and WT mice to label the endothelium in the mice of WT:TdTomato: iCdh5-Cre and EC-iDKO:TdTomato:iCdh5-Cre. All mice were given seven tamoxifen injections to activate the Tdtomato gene expression for the labeling of endothelial cells, followed by

WD feeding for 8 weeks. EndoMT marker SM22α was immunofluorescently stained in BCA (brachiocephalic artery) and aortic roots of WT and EC-iDKO mice. As shown in Figure 2, in the BCA of arch (A, B) and aortic roots (C, D), TdTomato gene expression (red color) co-localized with SM22α in EC-iDKO mice is significantly reduced when compared to WT mice, suggesting that endothelial epsins are necessary to promote EndoMT.

Loss of endothelial epsins attenuates EndoMT in atherosclerotic mice

Loss of epsins from the endothelium significantly reduced atherosclerotic plaques in the *Apoe*$^{-/-}$ mouse model, as demonstrated by Oil Red O (ORO) staining of the aortic root, arch, and BCA (Brachiocephalic artery) (Supplemental Figure 5), in line with our previous report[29]. Since EndoMT is critical for atherosclerosis, we measured EndoMT markers in aortic roots from *Apoe*$^{-/-}$ and EC-iDKO/*Apoe*$^{-/-}$ mice. As shown in Figure 3A & B, we co-stained CD31 with SMC markers αSMA and Myh11, the overlapping percentile between CD31 and SMC markers is much less in EC-iDKO/*Apoe*$^{-/-}$ mice than in *Apoe*$^{-/-}$ mice, suggesting that loss of endothelial epsins inhibited EndoMT. Similar results were obtained from the co-staining of CD31 with α-SM22 and Calponin in aortic roots (Supplemental Figure 6).

We then measured EndoMT markers in BCA region of arches. As shown in Figure 3C &D, the percentile of CD31 co-staining with SMC markers α-SMA and Myh11 were significantly reduced in EC-iDKO/*Apoe*$^{-/-}$ mice, analogous to the staining for SM22 and Calponin in iDKO/*Apoe*$^{-/-}$ mice (Supplemental Figure 7). Taken together, loss of endothelial epsins inhibits EndoMT in *Apoe*$^{-/-}$ mice.

Loss of epsins in endothelial cells attenuates the expression of EndoMT markers

Mouse primary cultured aortic endothelial cells (MAECs) were isolated as previously reported[29]. We measured EndoMT markers in MAECs from WT and EC-iDKO after treating with 10 ng/mL TGF-ß for 5 days, and our results demonstrated that VSMC and mesenchymal stem cell markers Acta2, N-cadherin, Collagen 1a and Fibronectin are significantly increased in WT MAECs, but not in EC-iDKO MAECs (Figure 4A, B), while

EC cell markers VE-cadherin and Claudin-5 is lower in WT MAECs, but higher in EC-iDKO MAECs in qPCR analysis (Figure 4C; see primers in Supplemental Table 1), further suggesting that epsins promote EndoMT.

Functionally, we measured cell migration using Transwell Migration Assay, EC-iDKO cells treated by TGFβ migrated less than WT MAECs inducted in 10% FBS chamber (Supplemental Figure 8).

Loss of endothelial epsins attenuates TGF-ß signaling *in vitro*

TGF-ß signaling has been proposed to be the main driver of EndoMT through phospho-Smad2 nucleus translocation[8, 11, 12, 14]. To this end, we measured TGF-ß signaling by TGF-ß-induced Smad2 translocation. As shown in Figure 4D & E, Smad2 translocation to nuclei by TGF-ß or oxLDL treatment is drastically inhibited in the EC-iDKO MAECs in immunofluorescent staining (Close-up view provided in the Supplemental Figure 9; also see antibody resources in Supplemental Table 2). To further confirm this result, we co-stained the TGF-ß signaling target gene Myh11 or αSMA with CD31, and we found that approximate 10.5% WT EC cells can be transformed from EC to SMC under TGF-ß treatment for a relatively longer period, while epsin loss in ECs strongly inhibited EndoMT (Figure 4F; Supplemental Figure 9 &10). Furthermore, we treated MAECs from WT and EC-iDKO mice with TGF-ß or oxLDL. TGF-ß signaling, indicative of phospho-Smad2, phospho-Smad1/5 as suggested by Cooley et al[37], and the target gene N-cadherin and Slug expression, are significantly reduced in MAECs of EC-iDKO compared to WT-MAECs in western blots (Figure 4G to 4J), in line with the results from immunofluorescence staining (Figure 4D to 4 F).

Loss of endothelial epsins attenuates TGF-ß signaling *in vivo*

Next, we measured downstream TGF-ß signaling activation in the brachiocephalic artery (BCA) of aortas from WT and EC-iDKO mice fed a WD for 2 months. We found that phospho-Smad2 and phospho-Smad1/5 [37], were significantly attenuated in the BCA region of endothelial epsin deficient mice (Figure 4K to 4M), while control mice fed a normal chow diet (ND) had no obvious TGF-ß signaling activation. These results are

consistent with our immunostaining of TGF-ß target genes such as αSMA, Myh11, SM22 and Calponin (co-stained with CD31) in aortic roots from *Apoe*$^{-/-}$ and EC-iDKO/*Apoe*$^{-/-}$ mice (Figure 3; Supplemental Figure 6 & 7). Taken together, loss of endothelial epsins inhibited TGF-ß signaling and EndoMT *in vitro* and *in vivo*.

Loss of epsins inhibits EndoMT through a UIM-dependent Epsin-FGFR1 interaction

FGFR1 is a well-characterized endogenous inhibitor of EndoMT [8, 11, 12, 14]. Consequently, we measured FGFR1 expression in the presence and absence of epsins. As we show in Fig 5A & B, loss of epsins in MAECs significantly upregulated FGFR1 expression, implying that loss of endothelial epsins physiologically blocks the endocytosis of FGFR1. Importantly, this phenomenon did not change in response to treatment with an inflammatory inducer of TGF-ß (2 ng/mL or 10 ng/mL), suggesting that epsins are required for the endocytosis of FGFR1, regardless of the physiological or pathological conditions. This result was confirmed in human aortic endothelial cells (HAECs) using epsin 1 and 2 siRNA (Figure 5C, D).

To evaluate the ability of epsins to directly bind FGFR1, we performed immunoprecipitation analyses. As shown in Figure 5E & F, FGFR1 can be co-immunoprecipitated with epsin 1 in wild type MAECs and *vice versa* (Figure 5G & H). To assess the plasma membrane (PM) FGFR1 levels, we biotinylated PM FGFR1 and precipitated these with a MagnaBind Streptavidin resin (Thermo Scientific). Our results show that loss of endothelial epsins stabilized PM FGFR1 (Figure 5I & J). Furthermore, we co-transfected HA-tagged Epsin1 or HA-tagged Epsin1-ΔUIM and Flag-tagged FGFR1 into WT MAECs by electroporation and immunoprecipitated these proteins with a FGFR1 antibody. We found that deletion of epsin UIM leads to abolition of epsin-FGFR1 interaction (Figure 5K to M; also see endogenous FGFR1 expression in Supplemental Figure 11). In other words, epsin UIM domain is critical for epsin-FGFR1 interaction.

Strategy to design a synthetic peptide to inhibit EndoMT *in vitro* and *in vivo*

We reasoned that an epsin-UIM-containing peptide would competitively interfere with the bind of epsins to FGFR1 to prevent its endocytosis and degradation (Figure 6A). We

synthesized an epsin UIM peptide, which was conjugated to an atheroma-specific targeting peptide sequence Lyp-1[38] at the N-terminus to form a chimeric peptide, named as API (Atheroma UIM Peptide Inhibitor) (Figure 6B). We first tested the peptide penetration capability in MAECs. Cells were pre-treated by 100 μg/mL oxLDL for 6h to create a "pro-inflammation" status, followed by the addition of FITC-conjugated API or control peptides. After 15h, cells were washed and images were taken under fluorescent microscopy. Our result demonstrates that only FITC-API, which contains the atheroma targeting peptide, can efficiently enter cells, but not FITC-UIM peptide (Figure 6C); suggesting that the leading peptide Lyp-1 is indispensable. Pretreatment of MAECs with API peptide considerably inhibited TGF-ß-induced EndoMT compared to control peptide (Figure 6D, E). This result is further supported by Smad2 immunostaining in control or API peptide preloaded MAECs (Figure 6F, G; close-up view provided in Supplemental Figure 12). API peptide pretreatment can significantly block the Smad2 translocation from cytoplasm to nuclei (Figure 6F, G).

We then tested the effect of API on EndoMT *in vivo*. We first examined the specific targeting of API peptide by injecting a FITC-conjugated API peptide into *Apoe*$^{-/-}$ mice fed a WD for 6 weeks. Four hours post-injection, mice were sacrificed and aortic roots were stained with DAPI. The API peptide was found to localize to atheroma, especially in the endothelium (Supplemental Figure 13). We compared EndoMT marker αSMA between *Apoe*$^{-/-}$ and EC-iDKO/*Apoe*$^{-/-}$ mice fed WD for 12 weeks. SMC markers αSMA overlapping with CD31 is significantly reduced in API peptide treated group, but rather control peptide group (Figure 6H), suggesting that API block endothelial cells transition to SMC, while FGFR1 is remarkably elevated in API treatment group, which in turn to inhibit TGF-ß signaling (Supplemental Figure 14), in line with our discovery in genetic mouse model, cell culture model and scRNA-seq data.

Perturbation of Epsin-FGFR1 interaction *in vivo* by API peptide impedes atherosclerotic progression in *Apoe*$^{-/-}$ mouse model: role of prevention

We then performed experiments to test the therapeutic efficacy of API in *Apoe*$^{-/-}$ atherosclerotic mouse model. In *Apoe*$^{-/-}$ atherosclerosis model, mice were injected with

API peptide by every-other-day at 50 mg/kg dosage and fed on WD for 2 months. Administration of API significantly inhibited atherosclerotic lesion development of aortic root (Figure 7A, B) and arch (Figure 7C and 7D). To further support our conclusion, we injected API to an alternative carotid atherosclerosis model. Expectedly, API peptide significantly attenuated atherosclerotic lesion development, associated with reduced macrophage infiltration (data not shown). Together, modulation of Epsin-FGFR1 interaction *in vivo* by API peptide is feasible and effective to inhibit EndoMT and atherosclerosis, mimicking the loss of EC epsin phenotype. This result implies a clinical potential to treat atherosclerosis by targeting epsins.

.

API peptide therapeutic efficacy in the lesion-established *Apoe*$^{-/-}$ mouse model: role of therapy

To determine the therapeutic potential of our candidate peptide compound, we established lesion-laden *Apoe*$^{-/-}$ mouse model by feeding *Apoe*$^{-/-}$ mice for 6 weeks on Western Diet (WD), then we started to inject control or API peptide to these lesion laden *Apoe*$^{-/-}$ model. As we can see in Figure 7E to Figure 7H, atherosclerotic plaques in API peptide treated group were significantly reduced in atherosclerotic lesions in aortic root and arches. A similar result was seen in BCA region of aortic arches (Figure 7I, J) as well as reduced macrophage infiltration detected by CD68 staining (Figure 7K, L). Together, these results suggest that the API peptide can not only prevent atherosclerosis, but also reverse in established atherosclerotic lesions (Figure 7).

In conclusion, we have identified a new molecular mechanism for epsin-modulated atherosclerosis through EndoMT, in which epsins potentiate endothelial-to-mesenchymal (*i.e.,* SMC) transition. A synthetic UIM-containing peptide (API) that interferes with epsin and FGFR1 interaction *in vivo* shows the potential to create a new class of therapeutics for the treatment of atherosclerosis (Figure 8).

DISCUSSION

Here, we demonstrate a novel role for epsins in potentiating EndoMT using *in vitro* and *in vivo* atherosclerotic models. Using epsin deficient mice, we discovered these endocytic adaptors regulate EndoMT in response to inflammatory stimuli and vascular disease, such as atherosclerosis[6].

Using scRNA-seq, epsin mutant mice, *Apoe*$^{-/-}$ model, lineage tracing mice and *in vitro* cell culture approaches, we demonstrate that epsins promote EndoMT (Figure1-4). Mechanistically, epsins modulate the protein levels of FGFR1 (Figure 5)—a well-documented endogenous inhibitor of EndoMT[8, 11, 12, 14]. Loss of endothelial epsins causes the accumulation of FGFR1 on the plasma membrane, which inhibits EndoMT under inflammatory conditions. This discovery expanded our understanding about the mechanism behind EndoMT and the complexity of atherosclerosis. Furthermore, epsins bind FGFR1 (Figure 5), which provides the therapeutic foundation to modulate EndoMT and atherosclerosis.

FGFR1 binds epsins via their UIM to enable receptor endocytosis in physiologically and pathologically circumstances (Figure 5). Conversely, the loss of endothelial epsins stabilizes cell surface FGFR1 (Figure 5), which is crucial for suppression of EndoMT. This finding is similar to our observations for VEGFR2 in neo-angiogenesis and tumor angiogenesis, both of which are dependent on UIM interactions between epsins and VEGF receptors[39, 40]. Interestingly, VEGFR2 has been reported to inhibit EndoMT[41], however, in large arteries like the aorta, VEGFR2 expression is minimal[23]. Therefore, the upregulation of FGFR1 in large vessels resulting from endothelial epsin loss may suppress EndoMT.

We previously reported that epsins bind to numerous receptors (*e.g.,* IP3R1, TNFR1, TLR2/4, and LRP1) via the UIM domain[30, 42-44]. This suggests that epsin UIM was a critical domain to regulate inflammatory receptors, which was the basis for the development of our therapeutic peptide. As a result, we designed an atheroma-targeting peptide called

API, in which a Lyp-1 transduction peptide was fused to the N-terminal of UIM sequence (Figure 6B).

Lyp-1 has been suggested to home to macrophage and p32 positive tumor cells, as well as tumor lymphatic vessels[38, 45, 46]. In our *in vitro* experiments, we found that a FITC-conjugated API peptide was efficiently taken up by MAECs pre-treated with oxLDL. In *Apoe*$^{-/-}$ mice, we visualized the FITC-conjugated API peptide homing to the atheroma (predominantly in the EC layer) (Supplemental Figure 13). In our proof-of-concept study, we provided evidence that atherosclerosis can be dramatically alleviated by downregulating EndoMT and upregulating FGFR1 expression using this atheroma targeted peptide (Supplemental Figure 14). Our data showed that atherosclerotic plaques can be significantly reduced by API peptide administration (Figure 7). However, we could not completely rule out the possibility that some of the API peptide targeted macrophages, which could provide additional anti-inflammatory benefits[30, 42-44].

Although EndoMT has been implicated in contributing to cardiovascular diseases, including atherosclerosis, pulmonary hypertension, tissue fibrosis and brain vascular malformation[6, 11, 47], a recent report suggests that EndoMT can transiently stabilize the atherosclerotic fibrous cap[9], reflecting that the role of EndoMT in atherosclerosis could be dual. The report showed convincingly that in murine and human lesions, 20% to 40% of the protective ACTA2+ myofibroblast (MF)-like cells in the fibrous cap, are actually derived from non-SMC sources, including endothelial cells (ECs) or macrophages that have undergone an endothelial-to-mesenchymal transition (EndoMT) or a macrophage-to-mesenchymal transition (MMT), respectively, suggesting that EndoMT is “protective” to plaque stabilization. However, in more advanced lesions, the beneficial role of EndoMT in plaque stabilization is diminished as PDGFβ signaling-mediated SMC recruitment to the fibrous cap is imperative to reinforce plaque stability. Thus, it is conceivable that EndoMT under aforesaid conditions would further fuel endothelial activation and dysfunction owing to prolonged loss of pool of endothelial cells that may be required for endothelial repair, crucial for maintaining endothelial homeostasis. Nevertheless, the role of endothelial epsins played in EndoMT on the stabilization of fibrous cap of

atherosclerosis warrants further investigation. Besides, EndoMT is required for heart mitral valve development and it is detectable for healthy adult valves in sheep and humans[48]. EndoMT can also be reactivated in the postnatal setting in both physiologically and pathologically states[49]. EndoMT has been proposed to be harmful to heart repair[50] , although it is still controversial if fibroblasts derived from EndoMT are responsible for the aforesaid events as recent studies show that a local pool of fibroblasts get reactivated and dynamically remodel following myocardial infarction injury, and lose SMA expression to maintain heart structure post myocardial infarction[51].

In summary, we demonstrated that the loss of epsins in endothelial cells inhibits atherosclerosis, at least in part, through inhibiting EndoMT. Mechanistically, epsins modulate FGFR1 expression and its endocytosis in atherosclerosis. Targeting atheroma-specific epsins by UIM-containing peptide API mitigates EndoMT and atherosclerosis (Figure 8). These findings are perspective to control atherosclerosis.

CLINICAL PERSPECTIVE

What Is New?

* Endothelial epsins are required for EndoMT *in vitro* and *in vivo*.
* Epsins interact with FGFR1 in a UIM-dependent fashion to govern FGFR1 endocytosis and degradation.
* Targeted delivery of a UIM-containing peptide (API) reduces atherosclerotic lesion size.

What Are the Clinical Implications?

* Targeting epsin-FGFR1 interaction with a therapeutic peptide is feasible means to reduce atherosclerotic plaque burden in mice.
* The homology of the UIM between humans and mice indicates this form of therapy could be used to treat atherosclerosis in patients.

FIGURE LEGENDS

Figure 1. Single cell RNA sequencing analysis reveals epsins are required for EndoMT.

A, **B**, Data quality control for WT and EC-iDKO cells in PCA and UMAP plots;

C, WT and EC-iDKO cells were clustered to 10 groups in UMAP visualization;

D, Representative makers for the labeling cell distribution in UMAP visualization for EndoMT models. *Col1a1* is specific to SMC and *Pecam1* to EC. SMC cells are excluded in consideration of the cell origin from the mouse blood vessels.

E, EC enriched cells (cluster 4) were further divided to 4 subgroups as indicated. The proportion of EC and Endothelial-to-Smooth Muscle Transition Cell (EST) types was identified (p=8.08e-13 by χ^2 test).

F, **G**, Violin plot of EC and SMC markers differentially expressed in WT and EC-iDKO in the endothelial subgroups of five EC marker positive cells (*Pecam1, Cdh5, Cldn5, Tek*, and *Notch1*) and five SMC maker positive cells (*Acta2, Tagln, Cald1, Mylk,* and *Col1a1*). *P* value is calculated via Wilcoxon test.

H, **I**, Gene expression tendencies of representative markers specific to EC (*Pecam1*) and SMC (*Tagln*) through EC-P^+/C^+-SMC axis of EndoMT shown as normalized expression versus UMAP_1 (also refer to the Supplemental Figure 4 with more maker genes).

J, **K**, Inference of pseudo-times for EndoMT trajectory from EC to SMC by *Slingshot*. A linear transition was identified from EC to SMC in aortas of mouse models.

Figure 2. Mouse lineage tracing suggests that epsins are crucial to promote EndoMT.

TdTomato mice of WT and EC-iDKO were all injected tamoxifen seven times and fed WD for 8 weeks. EndoMT marker SM22 was compared in BCA (brachiocephalic artery) (**A, B**) and aortic root (**C, D**) and quantified. n=5, *, ** P<0.001. Scale bar: 20 μm, and magnified: 10 μm.

Figure 3. EndoMT is attenuated in EC-iDKO/*Apoe*$^{-/-}$ mice.

A, **B**, Immunostaining of aortic roots with CD31 and EndoMT markers α-SMA (**A**), MyH11 (**B**) in *Apoe*$^{-/-}$ and EC-iDKO/*Apoe*$^{-/-}$ mice fed WD for 12 weeks. n=5 in each group, P value was indicated in the bar graph. Scale bar: 20 μm, and magnified: 10 μm.

C, **D**, Immunostaining of BCA with CD31 and EndoMT markers α-SMA (**C**), MyH11 **(D**) were co-stained with CD31 in *Apoe*$^{-/-}$ and EC-iDKO/*Apoe*$^{-/-}$ mice fed WD for 12 weeks. n=5 in each group, P value was indicated in the bar graph. Scale bar: 20 μm, and magnified: 10 μm.

Figure 4. Loss of endothelial epsins inhibits EndoMT via TGF-ß signaling *in vitro* and *in vivo*.

A to **C**, MAECs of WT and EC-iDKO were treated by 10 ng/mL TGF-ß for 2 days, change fresh medium and TGF-ß every-other-day, followed by qPCR to detect EndoMT markers. SMC markers Acta2, N-cadherin, Mesenchymal markers Collagen 1a, Fibronectin, endothelial markers VE-cadherin and Claudin-5 were measured respectively. n=3, *P<0.01.

D, **E**, Smad2 translocation was measured by immunofluorescent co-immunostaining Smad2 and Phalloidin-Flu 594. MAECs of WT and EC-iDKO were treated by 10 ng/mL TGF-ß or 100 μg/mL oxLDL for 5 days. n=5, P<0.001.

F, Co-immunostaining of CD31 and Myh11 for MAECs of WT and EC-iDKO treated by 10 ng/mL TGF-ß for a week. n=7, P<0.001. Scale bars: 50 μm for (**D**, **E**, **F**). Magnified in (**F**): 25 μm

G to **J**, MAECs of WT and EC-iDKO were treated by 10 ng/mL TGF-ß or 100 μg/mL oxLDL for 5 days, followed by western blot with specific antibodies for the phospho-Smad2 & phospho-Smad1/5 in TGF-ß signaling (**G**, **H**) and target gene expression (**I**, **J**).

K to **M**, TGF-ß signaling as indicated by phospho-Smad2 and phospho-Smad1/5 was measured in western blot from brachiocephalic artery (BCA) samples of WT and EC-iDKO fed western diet for 8 weeks. WT mice fed normal chow diet (ND) services as basal level controls. (**K**) Cartoon of the aortic region chosen for western blot in brachiocephalic artery. n=3 in each group. * WT/ND *vs* WT/WD, P<0.001; # WT/WD *vs* EC-iDKO/WD, P<0.001.

Figure 5. Endothelial epsins promote EndoMT by accelerating UIM-dependent FGFR1 endocytosis and degradation.

A, **B**, MAECs isolated from WT and Epsin1$^{f/f}$:Epsin2$^{-/-}$:iCDH5-cre mice were both treated with 5 μM tamoxifen for 5 days, followed by the treatment of 2 or 10 ng/mL TGF-ß for 3 days (maintain 1 μM tamoxifen during this stage). Cell lysates were subjected to western blot with specific antibody to FGFR1. n.s, no statistical difference. n=3, * P<0.001.

C, **D**, Epsin 1 and 2 were knockdown in human aortic endothelial cells (HAECs) by different concentration of siRNA, and cell lysates were subjected to western blot for FGFR1. n=3, * P<0.001.

E to **H**, Epsin 1 interacts with FGFR1 in reciprocal IP analysis. WT MAECs were cultured in complete EC medium and cell lysates were co-immunoprecipitated with Epsin1 (**E**) or FGFR1 (**G**). IgG as controls in co-IP experiment. Quantification is illustrated in (**F**) and (**H**) respectively. n=3, *, ** P<0.001.

I, **J**, Biotinylation of PM FGFR1 assay and western blotting for PM FGFR1. **I**, FGFR1 in PM; **J**, decay rate of FGFR1 in WT and EC-iDKO MAECs. n=3, P<0.001.

K to **M**, HA-tagged Epsin 1 or Epsin 1ΔUIM were co-transfected with FGFR1 plasmid into WT MAECs by electroporation (Lonza), after 36 hours, cell lysis was immunoprecipitated with FGFR1 antibody, followed by western blot with HA antibody. (**M**) Input for the IP analysis in (**K**). **L**, quantification for (**K**), n=3, † P<0.0001.

Figure 6. API peptide administration prevents TGF-ß signaling activation *in vitro* and in the *Apoe*$^{-/-}$ model.

A, Strategy for the design of a synthetic peptide API to competitively bind FGFR1 and block endogenous epsin binding

B, Peptide sequences used in this study

C, Co-incubation of 100 μg/mL oxLDL and 25 μM FITC-API or FITC-UIM for 15 h, cells were then fixed and stained with DAPI as reference. Images were captured under Olympus microscopy. Scale bar: 100 μm.

D, **E**, WT MAECs were pre-loaded with 50 μM control or API peptide, followed by the treatment of TGF-ß (10 ng/mL) as indicated time points. Phospho-Smad2 was measured in western blot and quantified (E). n=3, *P<0.001.

F, **G**, WT MAECs were pre-loaded with 50 μM control or API peptide, followed by the treatment of TGF-ß (10 ng/mL) for 3 days, and co-stained Smad2 nuclei translocation with Phalloidin-594 (**F**) and quantified (**G**). n=8, *P<0.001. Scale bar: 20 μm.

H, **I**, Control or API peptide treated mice for 12 weeks on WD was co-stained with CD31 and SMC markers α-SMA (**H**) and quantification (**I**), n=5 in each group, * P<0.01 in α-SMA. Scale bar: 200 μm (F), 20 μm (H).

Figure 7. API peptide therapy reduces atherosclerosis in the *Apoe*$^{-/-}$ mouse model.

A to **D**, Administration of API peptide significantly attenuated atherosclerosis in aortic roots (**A**, **B**) and aortic arches (**C**, **D**) in an *Apoe*$^{-/-}$ animal model. Peptide dose is 25 mg/kg, IV route, and twice a week. n=8 in each group; * or ** P<0.05. Scale bars: 500 μm (**A**); 5 mm (**C**).

E to **J**, API peptide treatment in lesion-laden *Apoe*$^{-/-}$ models blocked the progression of atherosclerosis. Age matched male *Apoe*$^{-/-}$ mice were fed WD for 6 weeks (sacrificed some mice as basal controls), and started to inject API peptide or control peptide (25 mg/kg, I. V. twice a week) for another 6 weeks, aortic roots (**E**, **F**), arches (**G**, **H**) and BCA (**I**, **J**) were stained with ORO and quantified. Basal control, n=3. Peptide injected group, n=5. P values were labelled in the bar graphs. Scale bar: 500 μm (**E**); 5 mm (**G**); 200 μm (**I**).

K, Macrophage infiltration staining by CD68 for aortic roots of basal control, control peptide and API peptide treatment groups. n=5, Ctr pep. *vs* pep., P=0.0063. Scale bar: 500 μm (**K**)

Figure 8. API administration inhibits EndoMT and atherosclerosis in *Apoe*$^{-/-}$ mouse model.

Under physiological conditions, Epsins bind FGFR1 via their UIM domain to promote endocytosis, resulting in receptor degradation in the lysosome. Under inflammatory conditions, internalization and degradation of FGFR1 facilitates EndoMT to potentiate atherosclerosis. Application of the synthetic API bind to FGFR1 competitively blocks the ability of endogenous epsins to bind FGFR1, which is replicates genetic epsin deficiency.

In both of the latter circumstances, FGFR1 remains at the plasma membrane to inhibit EndoMT induced by inflammation.

ACKNOWLEDGEMENTS

Y.D., B.W., and H.C. designed the experiments, analyzed and interpreted the data. Y.D. and B.W performed most of the experiments. M.D. analyzed the scRNA-seq data. B.Z. did the barcoding and cDNA library construction. K.C, S.B., and S.D. helped with immunostaining. S.W. performed the mouse genotyping and colony maintenance. Y.D., D.B.C., and H.C. wrote the manuscript. BGI-Hong Kong performed the scRNA-sequencing. M.L. and K.C. made constructive suggestions. We thank Dr. Yanqiang Li for his preliminary analysis of scRNA-seq data.

SOURCES OF FUNDING

This work was supported in part by the National Institute of Health (grants R01HL0093242-12, R01HL137229-04, R01HL1563626-01, R01HL158097-01, and R01HL146134-03 to H.C.).

DISCLOSURES

None

REFERENCES

1. Lusis AJ. Atherosclerosis. **Nature**. 2000; *407*:233-41. doi: 10.1038/35025203

2. Linton MRF, Yancey PG, Davies SS, Jerome WG, Linton EF, Song WL, Doran AC and Vickers KC. The Role of Lipids and Lipoproteins in Atherosclerosis. In: K. R. Feingold, B. Anawalt, A. Boyce, G. Chrousos, W. W. de Herder, K. Dhatariya, K. Dungan, J. M. Hershman, J. Hofland, S. Kalra, G. Kaltsas, C. Koch, P. Kopp, M. Korbonits, C. S. Kovacs, W. Kuohung, B. Laferrere, M. Levy, E. A. McGee, R. McLachlan, J. E. Morley, M. New, J. Purnell, R. Sahay, F. Singer, M. A. Sperling, C. A. Stratakis, D. L. Trence and D. P. Wilson, eds. *Endotext* South Dartmouth (MA); 2000 doi:

3. Dong Y, Fernandes C, Liu Y, Wu Y, Wu H, Brophy ML, Deng L, Song K, Wen A, Wong S, Yan D, Towner R and Chen H. Role of endoplasmic reticulum stress signalling in diabetic endothelial dysfunction and atherosclerosis. **Diab Vasc Dis Res**. 2017; *14*:14-23. doi: 10.1177/1479164116666762

4. Gimbrone MA, Jr. and Garcia-Cardena G. Endothelial Cell Dysfunction and the Pathobiology of Atherosclerosis. **Circ Res**. 2016; *118*:620-36. doi: 10.1161/CIRCRESAHA.115.306301

5. Hansson GK, Robertson AK and Soderberg-Naucler C. Inflammation and atherosclerosis. **Ann Rev Pathol**. 2006; *1*:297-329. doi: 10.1146/annurev.pathol.1.110304.100100

6. Chen PY, Qin L, Baeyens N, Li G, Afolabi T, Budatha M, Tellides G, Schwartz MA and Simons M. Endothelial-to-mesenchymal transition drives atherosclerosis progression. **J Clin Invest**. 2015; *125*:4514-28. doi: 10.1172/JCI82719

7. Souilhol C, Harmsen MC, Evans PC and Krenning G. Endothelial-mesenchymal transition in atherosclerosis. **Cardiovasc Res**. 2018; *114*:565-577. doi: 10.1093/cvr/cvx253

8. Chen PY, Qin L, Baeyens N, Li G, Afolabi T, Budatha M, Tellides G, Schwartz MA and Simons M. Endothelial-to-mesenchymal transition drives atherosclerosis progression. **J Clin Invest**. 2015; *125*:4514-28. doi: 10.1172/JCI82719

9. Newman AAC, Serbulea V, Baylis RA, Shankman LS, Bradley X, Alencar GF, Owsiany K, Deaton RA, Karnewar S, Shamsuzzaman S, Salamon A, Reddy MS, Guo L, Finn A, Virmani R, Cherepanova OA and Owens GK. Multiple cell types contribute to the atherosclerotic lesion fibrous cap by PDGFRbeta and bioenergetic mechanisms. **Nat Metab**. 2021; *3*:166-181. doi: 10.1038/s42255-020-00338-8

10. Evrard SM, Lecce L, Michelis KC, Nomura-Kitabayashi A, Pandey G, Purushothaman KR, d'Escamard V, Li JR, Hadri L, Fujitani K, Moreno PR, Benard L, Rimmele P, Cohain A, Mecham B, Randolph GJ, Nabel EG, Hajjar R, Fuster V, Boehm M and Kovacic JC. Endothelial to mesenchymal transition is common in atherosclerotic lesions and is associated with plaque instability. **Nat Commun**. 2016; *7*:11853. doi: 10.1038/ncomms11853

11. Chen PY, Schwartz MA and Simons M. Endothelial-to-Mesenchymal Transition, Vascular Inflammation, and Atherosclerosis. **Front Cardiovasc Med**. 2020; *7*:53. doi: 10.3389/fcvm.2020.00053

12. Chen PY, Qin L, Li G, Wang Z, Dahlman JE, Malagon-Lopez J, Gujja S, Cilfone NA, Kauffman KJ, Sun L, Sun H, Zhang X, Aryal B, Canfran-Duque A, Liu R, Kusters P, Sehgal A, Jiao Y, Anderson DG, Gulcher J, Fernandez-Hernando C, Lutgens E, Schwartz MA, Pober JS, Chittenden TW, Tellides G and Simons M. Endothelial TGF-beta signalling drives vascular inflammation and atherosclerosis. **Nat Metab**. 2019; *1*:912-926. doi: 10.1038/s42255-019-0102-3

13. Howe KL and Fish JE. Transforming endothelial cells in atherosclerosis. **Nat Metab**. 2019; *1*:856-857. doi: 10.1038/s42255-019-0100-5

14. Chen PY, Qin L, Tellides G and Simons M. Fibroblast growth factor receptor 1 is a key inhibitor of TGFbeta signaling in the endothelium. **Sci Signal**. 2014; *7*:ra90. doi: 10.1126/scisignal.2005504

15. Dal-Bianco JP, Aikawa E, Bischoff J, Guerrero JL, Hjortnaes J, Beaudoin J, Szymanski C, Bartko PE, Seybolt MM, Handschumacher MD, Sullivan S, Garcia ML, Mauskapf A, Titus JS, Wylie-Sears J, Irvin WS, Chaput M, Messas E, Hagege AA, Carpentier A and Levine RA. Myocardial Infarction Alters Adaptation of the Tethered Mitral Valve. **J Am Coll Cardiol**. 2016; *67*:275-87. doi: 10.1016/j.jacc.2015.10.092

16. Dal-Bianco JP, Aikawa E, Bischoff J, Guerrero JL, Handschumacher MD, Sullivan S, Johnson B, Titus JS, Iwamoto Y, Wylie-Sears J, Levine RA and Carpentier A. Active adaptation of the tethered mitral valve: insights into a compensatory mechanism for functional mitral regurgitation. **Circulation**. 2009; *120*:334-42. doi: 10.1161/CIRCULATIONAHA.108.846782

17. Min D and Popovic ZB. Mitral Valve Adaptation in Ischemic Heart Disease. **J Am Coll Cardiol**. 2016; *67*:288-90. doi: 10.1016/j.jacc.2015.11.036

18. Man S, Sanchez Duffhues G, Ten Dijke P and Baker D. The therapeutic potential of targeting the endothelial-to-mesenchymal transition. **Angiogenesis**. 2019; *22*:3-13. doi: 10.1007/s10456-018-9639-0

19. Bartko PE, Dal-Bianco JP, Guerrero JL, Beaudoin J, Szymanski C, Kim DH, Seybolt MM, Handschumacher MD, Sullivan S, Garcia ML, Titus JS, Wylie-Sears J, Irvin WS, Messas E, Hagege AA, Carpentier A, Aikawa E, Bischoff J and Levine RA. Effect of Losartan on Mitral Valve Changes After Myocardial Infarction. **J Am Coll Cardiol**. 2017; *70*:1232-1244. doi: 10.1016/j.jacc.2017.07.734

20. Pierard LA and Magne J. New Pharmacological Target to Treat Ischemic Mitral Regurgitation: Thinking Outside the Box. **J Am Coll Cardiol**. 2017; *70*:1245-1247. doi: 10.1016/j.jacc.2017.07.751

21. Chen H, Fre S, Slepnev VI, Capua MR, Takei K, Butler MH, Di Fiore PP and De Camilli P. Epsin is an EH-domain-binding protein implicated in clathrin-mediated endocytosis. **Nature**. 1998; *394*:793-7. doi: 10.1038/29555

22. Ford MG, Mills IG, Peter BJ, Vallis Y, Praefcke GJ, Evans PR and McMahon HT. Curvature of clathrin-coated pits driven by epsin. **Nature**. 2002; *419*:361-6. doi: 10.1038/nature01020

23. Dong Y, Wu H, Rahman HN, Liu Y, Pasula S, Tessneer KL, Cai X, Liu X, Chang B, McManus J, Hahn S, Dong J, Brophy ML, Yu L, Song K, Silasi-Mansat R, Saunders D, Njoku C, Song H, Mehta-D'Souza P, Towner R, Lupu F, McEver RP, Xia L, Boerboom D, Srinivasan RS and Chen H. Motif mimetic of epsin perturbs tumor growth and metastasis. **J Clin Invest**. 2015; *125*:4349-64. doi: 10.1172/JCI80349

24. Liu X, Pasula S, Song H, Tessneer KL, Dong Y, Hahn S, Yago T, Brophy ML, Chang B, Cai X, Wu H, McManus J, Ichise H, Georgescu C, Wren JD, Griffin C, Xia L, Srinivasan RS and Chen H. Temporal and spatial regulation of epsin abundance and VEGFR3 signaling are required for lymphatic valve formation and function. **Sci Signal**. 2014; *7*:ra97. doi: 10.1126/scisignal.2005413

25. Pasula S, Cai X, Dong Y, Messa M, McManus J, Chang B, Liu X, Zhu H, Mansat RS, Yoon SJ, Hahn S, Keeling J, Saunders D, Ko G, Knight J, Newton G, Luscinskas F, Sun X, Towner R, Lupu F, Xia L, Cremona O, De Camilli P, Min W and Chen H. Endothelial epsin deficiency decreases tumor growth by enhancing VEGF signaling. **J Clin Invest**. 2012; *122*:4424-38. doi: 10.1172/JCI64537

26. Rahman HNA, Wu H, Dong Y, Pasula S, Wen A, Sun Y, Brophy ML, Tessneer KL, Cai X, McManus J, Chang B, Kwak S, Rahman NS, Xu W, Fernandes C, McDaniel JM, Xia L, Smith L, Srinivasan RS and Chen H. Selective Targeting of a Novel Epsin-VEGFR2 Interaction Promotes VEGF-Mediated Angiogenesis. **Circ Res**. 2016; *118*:957-969. doi: 10.1161/CIRCRESAHA.115.307679

27. Tessneer KL, Pasula S, Cai X, Dong Y, McManus J, Liu X, Yu L, Hahn S, Chang B, Chen Y, Griffin C, Xia L, Adams RH and Chen H. Genetic reduction of vascular endothelial growth factor receptor 2 rescues aberrant angiogenesis caused by epsin deficiency. **Arterioscler Thromb Vasc Biol**. 2014; *34*:331-7. doi: 10.1161/ATVBAHA.113.302586

28. Chen H, Ko G, Zatti A, Di Giacomo G, Liu L, Raiteri E, Perucco E, Collesi C, Min W, Zeiss C, De Camilli P and Cremona O. Embryonic arrest at midgestation and disruption of Notch signaling produced by the absence of both epsin 1 and epsin 2 in mice. **Proc Natl Acad Sci U S A**. 2009; *106*:13838-43. doi: 10.1073/pnas.0907008106

29. Dong Y, Lee Y, Cui K, He M, Wang B, Bhattacharjee S, Zhu B, Yago T, Zhang K, Deng L, Ouyang K, Wen A, Cowan DB, Song K, Yu L, Brophy ML, Liu X, Wylie-Sears J, Wu H, Wong S, Cui G, Kawashima Y, Matsumoto H, Kodera Y, Wojcikiewicz RJH, Srivastava S, Bischoff J, Wang DZ, Ley K and Chen H. Epsin-mediated degradation of IP3R1 fuels atherosclerosis. **Nat Commun**. 2020; *11*:3984. doi: 10.1038/s41467-020-17848-4

30. Dong Y, Wang B, Cui K, Cai X, Bhattacharjee S, Wong S, Cowan DB and Chen H. Epsins Negatively Regulate Aortic Endothelial Cell Function by Augmenting Inflammatory Signaling. **Cells**. 2021; *10* doi: 10.3390/cells10081918

31. Brophy ML, Dong Y, Tao H, Yancey PG, Song K, Zhang K, Wen A, Wu H, Lee Y, Malovichko MV, Sithu SD, Wong S, Yu L, Kocher O, Bischoff J, Srivastava S, Linton MF, Ley K and Chen H. Myeloid-Specific Deletion of Epsins 1 and 2 Reduces Atherosclerosis by Preventing LRP-1 Downregulation. **Circ Res**. 2019; *124*:e6-e19. doi: 10.1161/CIRCRESAHA.118.313028

32. Dong Y, Zhang M, Wang S, Liang B, Zhao Z, Liu C, Wu M, Choi HC, Lyons TJ and Zou MH. Activation of AMP-activated protein kinase inhibits oxidized LDL-triggered endoplasmic reticulum stress in vivo. **Diabetes**. 2010; *59*:1386-96. doi: 10.2337/db09-1637

33. Dong Y, Zhang M, Liang B, Xie Z, Zhao Z, Asfa S, Choi HC and Zou MH. Reduction of AMP-activated protein kinase alpha2 increases endoplasmic reticulum stress and atherosclerosis in vivo. **Circulation**. 2010; *121*:792-803. doi: 10.1161/CIRCULATIONAHA.109.900928

34. Butler A, Hoffman P, Smibert P, Papalexi E and Satija R. Integrating single-cell transcriptomic data across different conditions, technologies, and species. **Nat Biotechnol**. 2018; *36*:411-420. doi: 10.1038/nbt.4096

35. Street K, Risso D, Fletcher RB, Das D, Ngai J, Yosef N, Purdom E and Dudoit S. Slingshot: cell lineage and pseudotime inference for single-cell transcriptomics. **BMC Genomics**. 2018; *19*:477. doi: 10.1186/s12864-018-4772-0

36. Wang B, Zhang L, Liu J, Ma L, Wang H, Zheng N, Chen X, Shen B and Xu Z. Chlamydia pneumoniae infection promotes vascular endothelial cell angiogenesis through an IQGAP1-related signaling pathway. **Int J Med Microbiol**. 2017; *307*:276-286. doi: 10.1016/j.ijmm.2017.03.001

37. Cooley BC, Nevado J, Mellad J, Yang D, St Hilaire C, Negro A, Fang F, Chen G, San H, Walts AD, Schwartzbeck RL, Taylor B, Lanzer JD, Wragg A, Elagha A, Beltran LE, Berry C, Feil R, Virmani R, Ladich E, Kovacic JC and Boehm M. TGF-beta signaling mediates endothelial-to-mesenchymal transition (EndMT) during vein graft remodeling. **Sci Transl Med**. 2014; *6*:227ra34. doi: 10.1126/scitranslmed.3006927

38. Hamzah J, Kotamraju VR, Seo JW, Agemy L, Fogal V, Mahakian LM, Peters D, Roth L, Gagnon MK, Ferrara KW and Ruoslahti E. Specific penetration and accumulation of a homing peptide within atherosclerotic plaques of apolipoprotein E-deficient mice. **Proc Natl Acad Sci U S A**. 2011; *108*:7154-9. doi: 10.1073/pnas.1104540108

39. Klauber-Demore N. Are epsins a therapeutic target for tumor angiogenesis? **J Clin Invest**. 2012; *122*:4341-3. doi: 10.1172/JCI66171

40. Pasula S, Cai X, Dong Y, Messa M, McManus J, Chang B, Liu X, Zhu H, Mansat RS, Yoon SJ, Hahn S, Keeling J, Saunders D, Ko G, Knight J, Newton G, Luscinskas F, Sun X, Towner R, Lupu F, Xia L, Cremona O, De Camilli P, Min W and Chen H. Endothelial epsin deficiency decreases tumor growth by enhancing VEGF signaling. **J Clin Invest**. 2012; *122*:4424-38. doi: 10.1172/JCI64537

41. Paruchuri S, Yang JH, Aikawa E, Melero-Martin JM, Khan ZA, Loukogeorgakis S, Schoen FJ and Bischoff J. Human pulmonary valve progenitor cells exhibit endothelial/mesenchymal plasticity in response to vascular endothelial growth factor-A and transforming growth factor-beta2. **Circ Res**. 2006; *99*:861-9. doi: 10.1161/01.RES.0000245188.41002.2c

42. Dong Y, Lee Y, Cui K, He M, Wang B, Bhattacharjee S, Zhu B, Yago T, Zhang K, Deng L, Ouyang K, Wen A, Cowan DB, Song K, Yu L, Brophy ML, Liu X, Wylie-Sears J, Wu H, Wong S, Cui G, Kawashima Y, Matsumoto H, Kodera Y, Wojcikiewicz RJH, Srivastava S, Bischoff J, Wang DZ, Ley K and Chen H. Epsin-mediated degradation of IP3R1 fuels atherosclerosis. **Nat Commun**. 2020; *11*:3984. doi: 10.1038/s41467-020-17848-4

43. Brophy ML, Dong Y, Tao H, Yancey PG, Song K, Zhang K, Wen A, Wu H, Lee Y, Malovichko MV, Sithu SD, Wong S, Yu L, Kocher O, Bischoff J, Srivastava S, Linton MF, Ley K and Chen H. Myeloid-Specific Deletion of Epsins 1 and 2 Reduces Atherosclerosis by Preventing LRP-1 Downregulation. **Circ Res**. 2019; *124*:e6-e19. doi: 10.1161/CIRCRESAHA.118.313028

44. Song K, Cai X, Dong Y, Wu H, Wei Y, Shankavaram UT, Cui K, Lee Y, Zhu B, Bhattacharjee S, Wang B, Zhang K, Wen A, Wong S, Yu L, Xia L, Welm AL, Bielenberg DR, Camphausen KA, Kang Y and Chen H. Epsins 1 and 2 promote NEMO linear ubiquitination via LUBAC to drive breast cancer development. **J Clin Invest**. 2021; *131* doi: 10.1172/JCI129374

45. Fogal V, Zhang L, Krajewski S and Ruoslahti E. Mitochondrial/cell-surface protein p32/gC1qR as a molecular target in tumor cells and tumor stroma. **Cancer Res**. 2008; *68*:7210-8. doi: 10.1158/0008-5472.CAN-07-6752

46. Laakkonen P, Porkka K, Hoffman JA and Ruoslahti E. A tumor-homing peptide with a targeting specificity related to lymphatic vessels. **Nat Med**. 2002; *8*:751-5. doi: 10.1038/nm720

47. Hulshoff MS, Del Monte-Nieto G, Kovacic J and Krenning G. Non-coding RNA in endothelial-to-mesenchymal transition. **Cardiovasc Res**. 2019; *115*:1716-1731. doi: 10.1093/cvr/cvz211

48. Bischoff J. Endothelial-to-Mesenchymal Transition. **Circ Res**. 2019; *124*:1163-1165. doi: 10.1161/CIRCRESAHA.119.314813

49. Kovacic JC, Dimmeler S, Harvey RP, Finkel T, Aikawa E, Krenning G and Baker AH. Endothelial to Mesenchymal Transition in Cardiovascular Disease: JACC State-of-the-Art Review. **J Am Coll Cardiol**. 2019; *73*:190-209. doi: 10.1016/j.jacc.2018.09.089

50. Li Y, Lui KO and Zhou B. Reassessing endothelial-to-mesenchymal transition in cardiovascular diseases. **Nat Rev Cardiol**. 2018; *15*:445-456. doi: 10.1038/s41569-018-0023-y

51. Fu X, Khalil H, Kanisicak O, Boyer JG, Vagnozzi RJ, Maliken BD, Sargent MA, Prasad V, Valiente-Alandi I, Blaxall BC and Molkentin JD. Specialized fibroblast differentiated states underlie scar formation in the infarcted mouse heart. **J Clin Invest**. 2018; *128*:2127-2143. doi: 10.1172/JCI98215

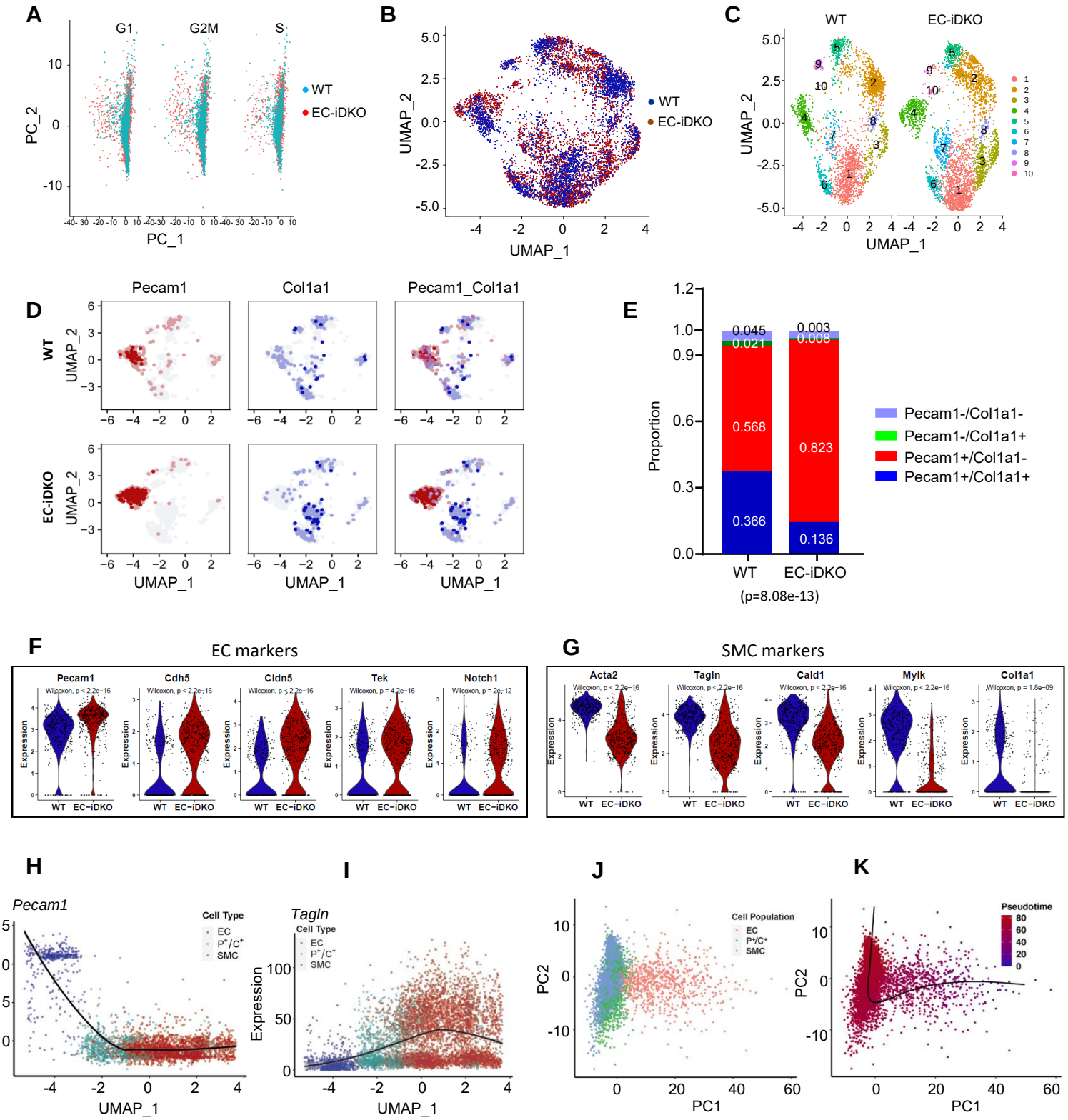
A
G1
G2M
S
PC_2
PC_1
WT
EC-iDKO
B
UMAP_2
UMAP_1
WT
EC-iDKO
C
WT
EC-iDKO
UMAP_2
UMAP_1
D
Pecam1
Col1a1
Pecam1_Col1a1
WT
EC-iDKO
UMAP_2
UMAP_1
E
Proportion
0.045
0.021
0.568
0.366
0.003
0.008
0.823
0.136
WT
EC-iDKO
(p=8.08e-13)
Pecam1-/Col1a1-
Pecam1-/Col1a1+
Pecam1+/Col1a1-
Pecam1+/Col1a1+
F
EC markers
Pecam1
Cdh5
Cldn5
Tek
Notch1
Expression
WT
EC-iDKO
G
SMC markers
Acta2
Tagln
Cald1
Mylk
Col1a1
Expression
WT
EC-iDKO
H
Pecam1
Cell Type
EC
P+/C+
SMC
Expression
UMAP_1
I
Tagln
Cell Type
EC
P+/C+
SMC
Expression
UMAP_1
J
Cell Population
EC
P+/C+
SMC
PC2
PC1
K
Pseudotime
80
60
40
20
0
PC2
PC1

Figure 1.

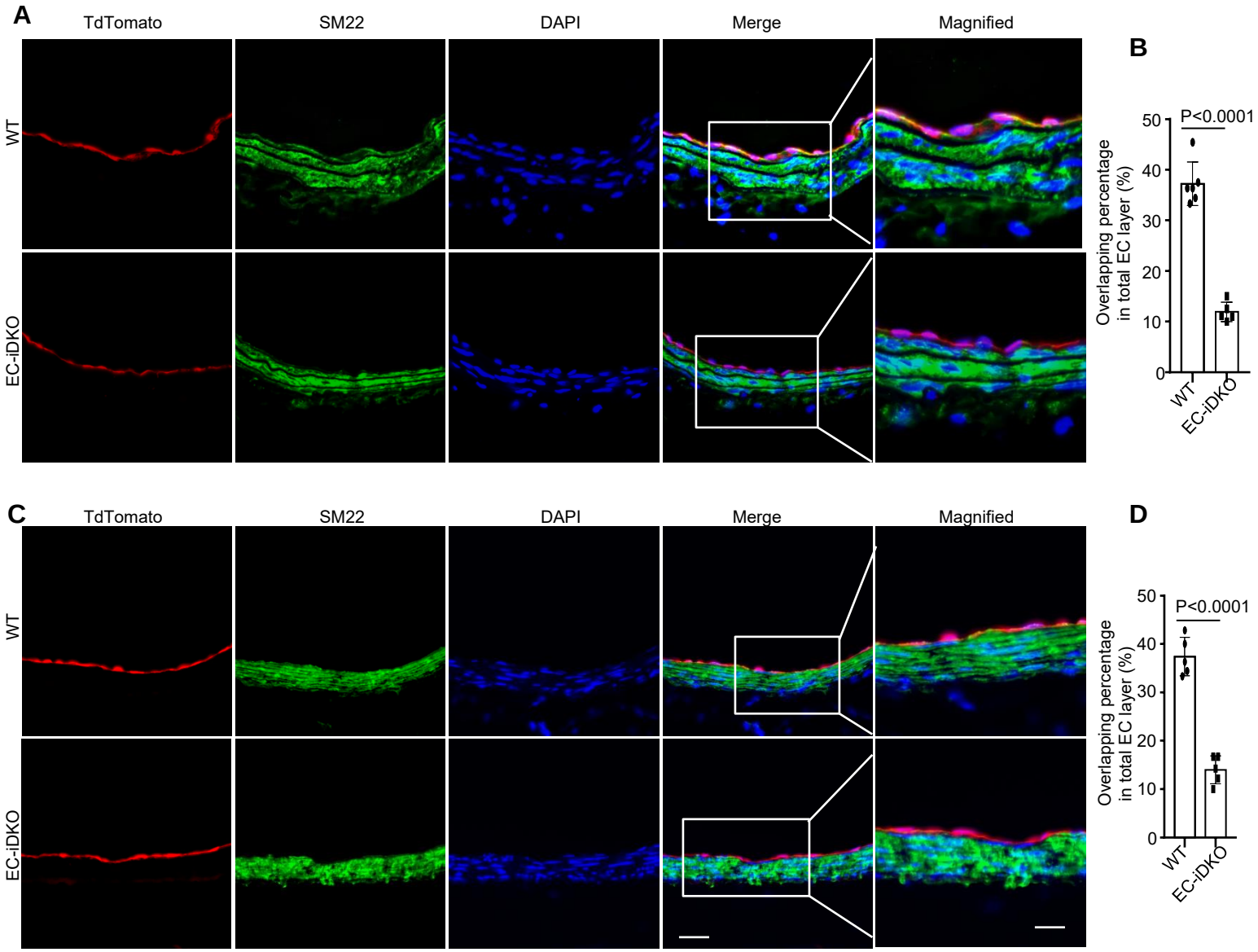
A
TdTomato
SM22
DAPI
Merge
Magnified
WT
EC-iDKO
B
P<0.0001
Overlapping percentage in total EC layer (%)
50
40
30
20
10
0
WT
EC-iDKO
C
TdTomato
SM22
DAPI
Merge
Magnified
WT
EC-iDKO
D
P<0.0001
Overlapping percentage in total EC layer (%)
50
40
30
20
10
0
WT
EC-iDKO

Figure 2.

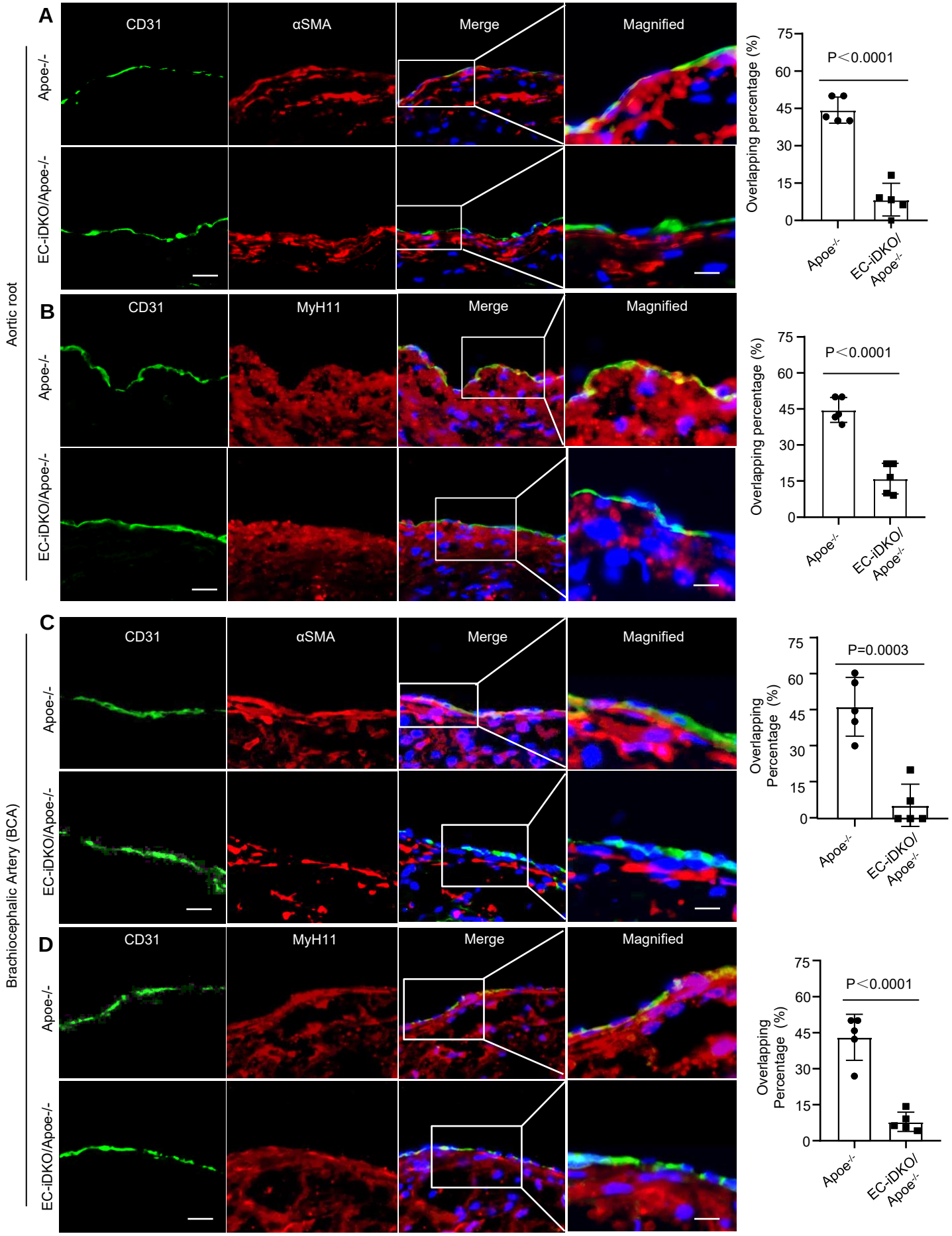
A
CD31
αSMA
Merge
Magnified
Apoe-/-
EC-iDKO/Apoe-/-
Aortic root
Overlapping percentage (%)
P<0.0001
Apoe-/-
EC-iDKO/ Apoe-/-
B
CD31
MyH11
Merge
Magnified
Apoe-/-
EC-iDKO/Apoe-/-
Overlapping percentage (%)
P<0.0001
Apoe-/-
EC-iDKO/ Apoe-/-
C
CD31
αSMA
Merge
Magnified
Apoe-/-
EC-iDKO/Apoe-/-
Brachiocephalic Artery (BCA)
Overlapping Percentage (%)
P=0.0003
Apoe-/-
EC-iDKO/ Apoe-/-
D
CD31
MyH11
Merge
Magnified
Apoe-/-
EC-iDKO/Apoe-/-
Overlapping Percentage (%)
P<0.0001
Apoe-/-
EC-iDKO/ Apoe-/-

Figure 3.

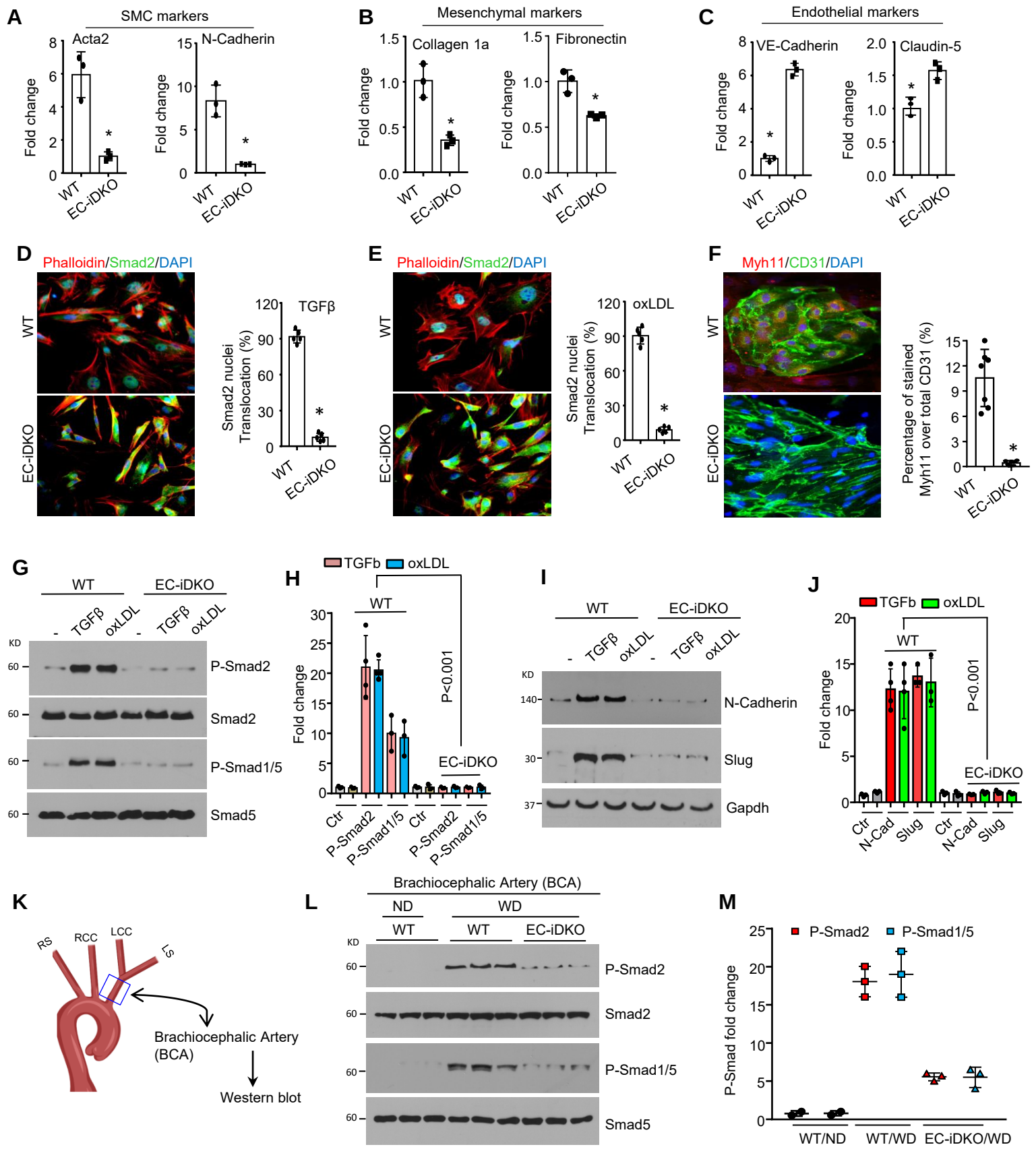
A
SMC markers
Acta2
N-Cadherin
Fold change
WT
EC-iDKO
B
Mesenchymal markers
Collagen 1a
Fibronectin
C
Endothelial markers
VE-Cadherin
Claudin-5
D
Phalloidin/Smad2/DAPI
TGFβ
Smad2 nuclei Translocation (%)
E
oxLDL
F
Myh11/CD31/DAPI
Percentage of stained Myh11 over total CD31 (%)
G
P-Smad2
Smad2
P-Smad1/5
Smad5
H
TGFb
oxLDL
P<0.001
Ctr
I
N-Cadherin
Slug
Gapdh
J
K
RS
RCC
LCC
LS
Brachiocephalic Artery (BCA)
Western blot
L
Brachiocephalic Artery (BCA)
ND
WD
M
P-Smad2
P-Smad1/5
P-Smad fold change
WT/ND
WT/WD
EC-iDKO/WD

Figure 4.

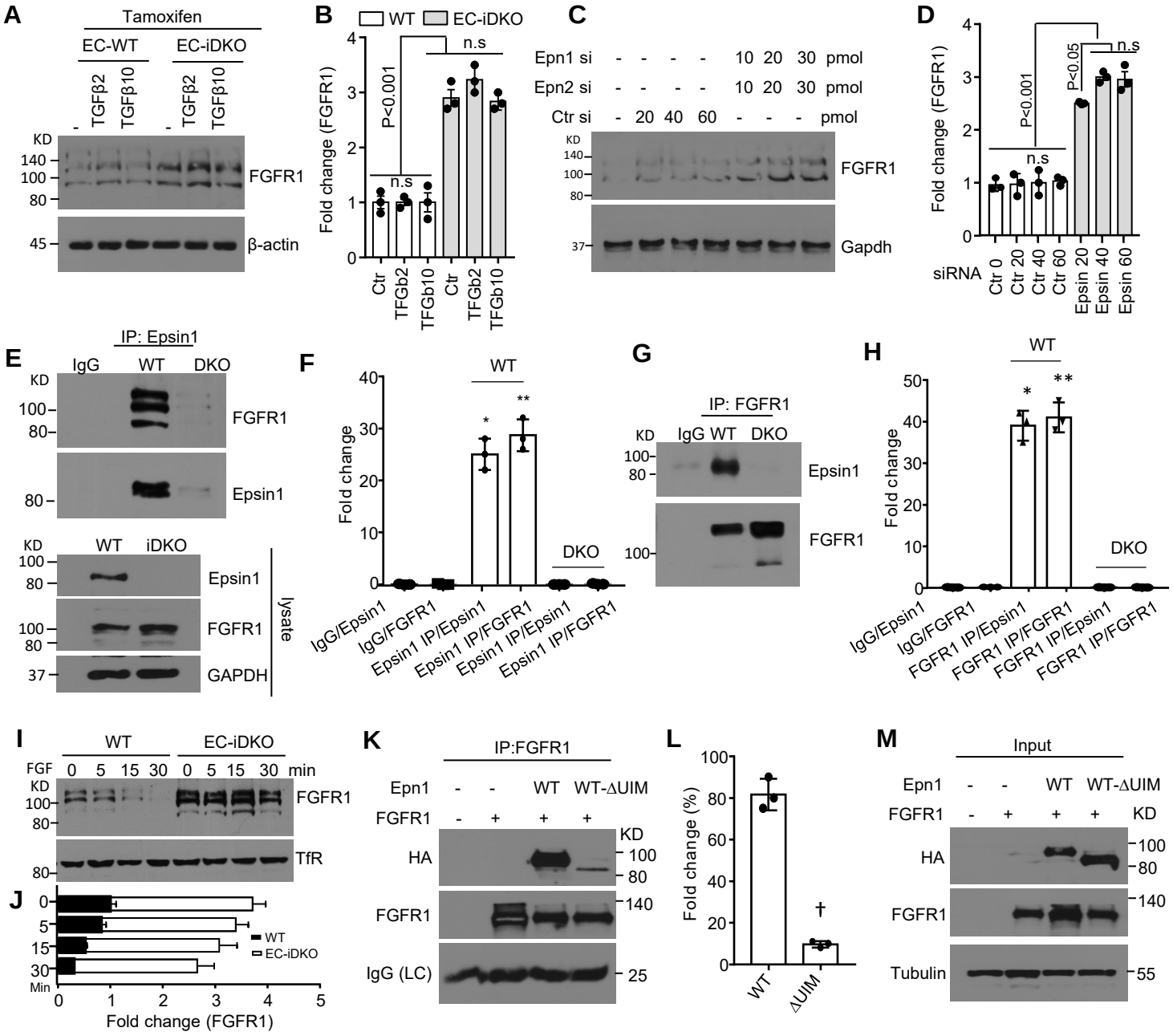
A
Tamoxifen
EC-WT
EC-iDKO
TGFβ2
TGFβ10
KD
140
100
80
FGFR1
45
β-actin
B
WT
EC-iDKO
Fold change (FGFR1)
P<0.001
n.s
Ctr
TFGb2
TFGb10
C
Epn1 si
Epn2 si
Ctr si
pmol
FGFR1
37
Gapdh
D
Fold change (FGFR1)
P<0.001
P<0.05
n.s
siRNA
Ctr 0
Ctr 20
Ctr 40
Ctr 60
Epsin 20
Epsin 40
Epsin 60
E
IP: Epsin1
IgG
WT
DKO
FGFR1
Epsin1
iDKO
lysate
GAPDH
F
Fold change
IgG/Epsin1
IgG/FGFR1
Epsin1 IP/Epsin1
Epsin1 IP/FGFR1
G
IP: FGFR1
H
FGFR1 IP/Epsin1
FGFR1 IP/FGFR1
I
FGF
min
TfR
J
Min
Fold change (FGFR1)
K
IP:FGFR1
Epn1
WT-ΔUIM
HA
IgG (LC)
L
Fold change (%)
ΔUIM
M
Input
Tubulin

Figure 5.

A

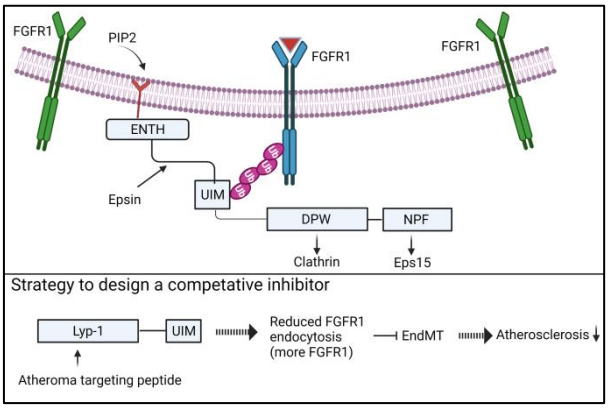

B

Peptides	Sequence	# of amino acids
Control	CGNKRTRGCQSLQESGMELEAELALEK	27
API	CGNKRTRGCSGEEELQLQLALAMSKEE	27
Cell targeting control	FITC-SGEEELQLQLALAMSKEE	18 (* without Lyp-1 leading peptide)
FITC-API	FITC-CGNKRTRGCSGEEELQLQLALAMSKEE	27

Lyp-1: CGNKRTRGC, leading peptide to atheroma; a ligand to p32 receptor;
Red: UIM sequence of epsins;
Blue: scrambled UIM sequence
API: Athroma UIM Peptide Inhibitor

C

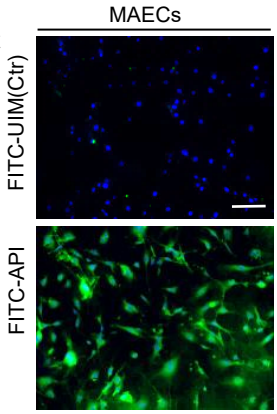

D

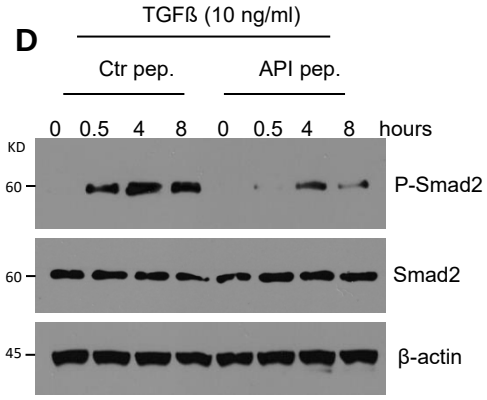

E

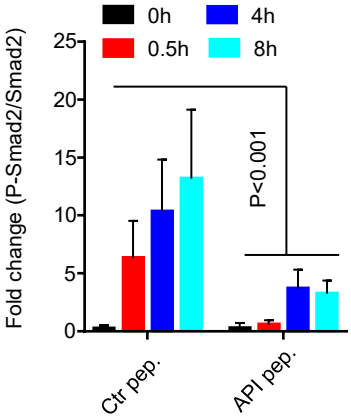

F

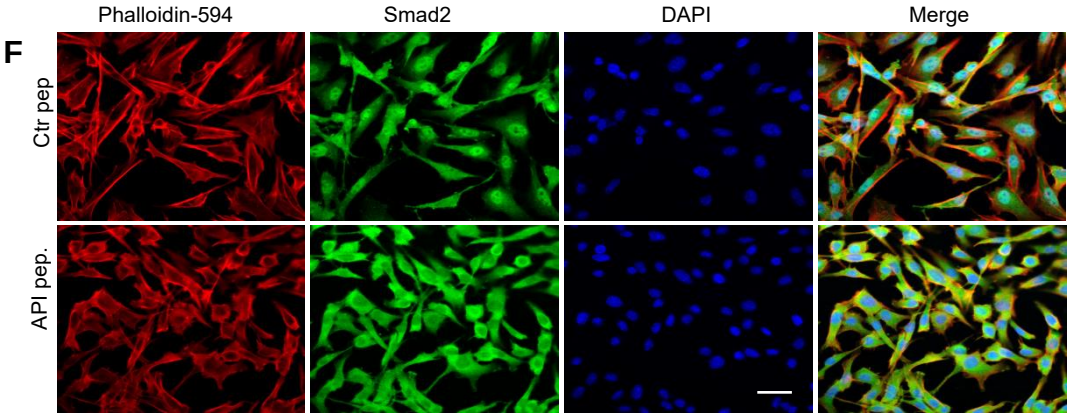

G

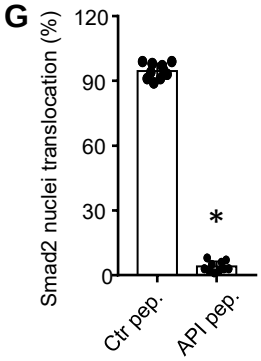

H

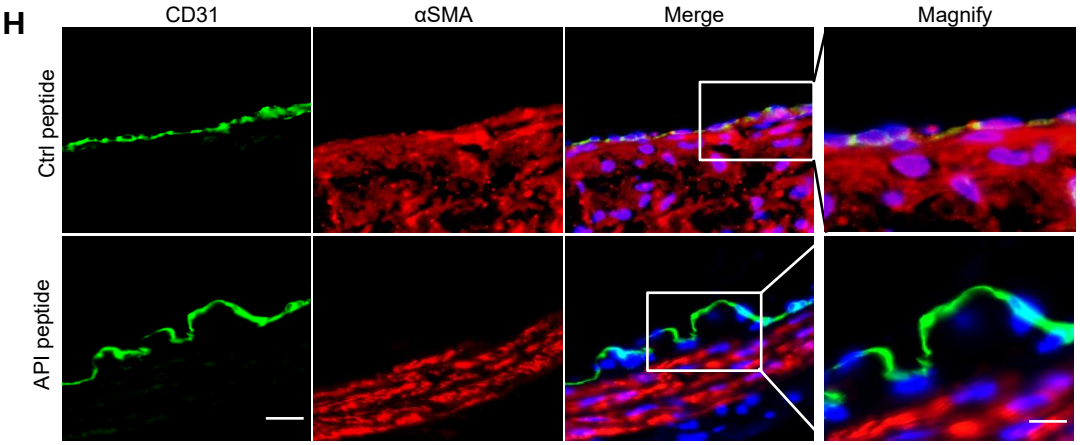

I

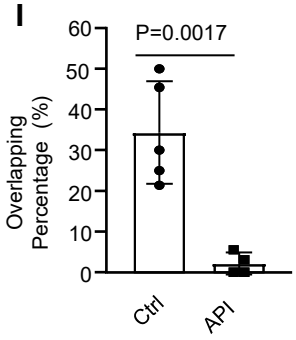

Figure 6.

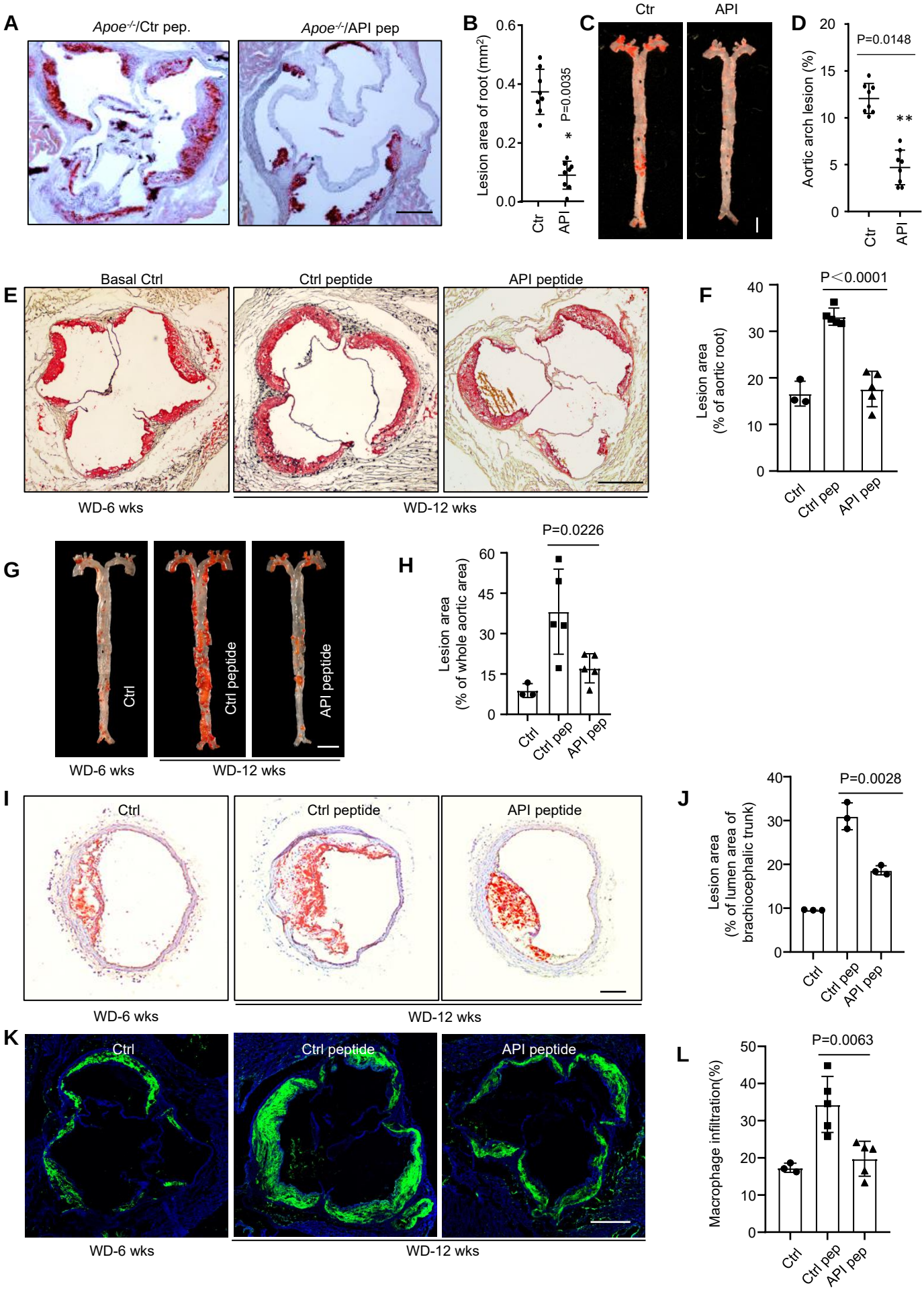
A
Apoe-/-/Ctr pep.
Apoe-/-/API pep
B
Lesion area of root (mm2)
P=0.0035
*
Ctr
API
C
Ctr
API
D
Aortic arch lesion (%)
P=0.0148
**
Ctr
API
E
Basal Ctrl
Ctrl peptide
API peptide
WD-6 wks
WD-12 wks
F
Lesion area (% of aortic root)
P<0.0001
Ctrl
Ctrl pep
API pep
G
Ctrl
Ctrl peptide
API peptide
WD-6 wks
WD-12 wks
H
Lesion area (% of whole aortic area)
P=0.0226
Ctrl
Ctrl pep
API pep
I
Ctrl
Ctrl peptide
API peptide
WD-6 wks
WD-12 wks
J
Lesion area (% of lumen area of brachiocephalic trunk)
P=0.0028
Ctrl
Ctrl pep
API pep
K
Ctrl
Ctrl peptide
API peptide
WD-6 wks
WD-12 wks
L
Macrophage infiltration(%)
P=0.0063
Ctrl
Ctrl pep
API pep

Figure 7.

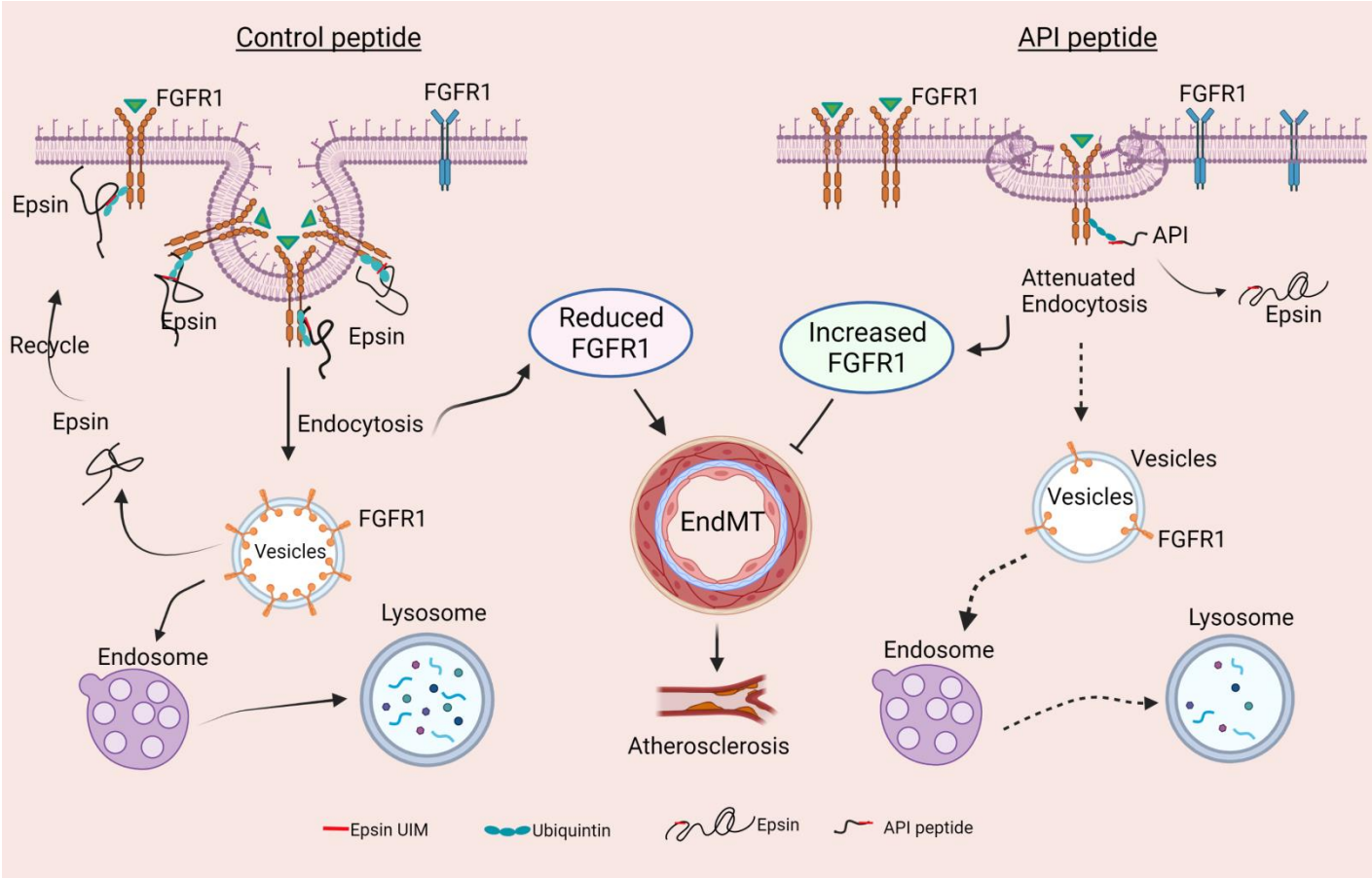
Control peptide
API peptide
FGFR1
FGFR1
Epsin
Epsin
Epsin
Recycle
Epsin
Endocytosis
Reduced FGFR1
Increased FGFR1
FGFR1
FGFR1
API
Attenuated Endocytosis
Epsin
Vesicles
FGFR1
Vesicles
Vesicles
FGFR1
EndMT
Endosome
Lysosome
Endosome
Lysosome
Atherosclerosis
Epsin UIM
Ubiquintin
Epsin
API peptide

Figure 8.

Supplemental Figures and Tables

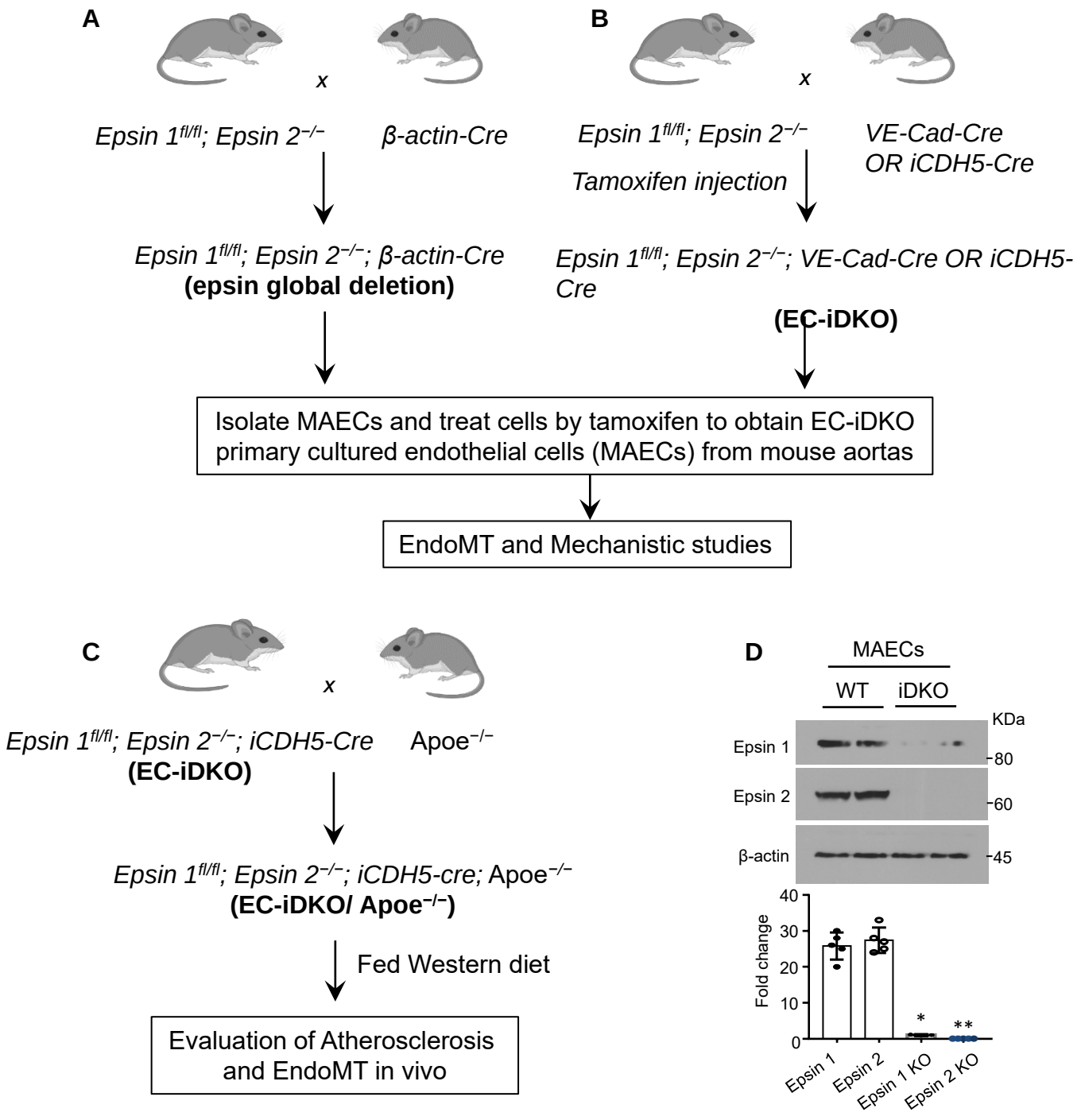

Supplemental Figure 1. **Procedures to generate primary cultured mouse endothelial cells (MAECs)from mouse aortas and epsin mutant mice in Apoe-null murine atherosclerosis model.**
(**A**) Global epsin DKO under constitutive β-actin driven Cre. (**B**) conditional DKO epsins in endothelium Driven by VE-Cadherin promoter. (**C**) generating epsin DKO mice in Apoe-null mouse model. (**D**) creation of epsins DKO MAECs in petri dishes. Isolated cells were treated by 5 μM tamoxifen for 4 days, followed by western blot analysis. VE: vascular endothelium. n=3. *, ** P<0.0001.

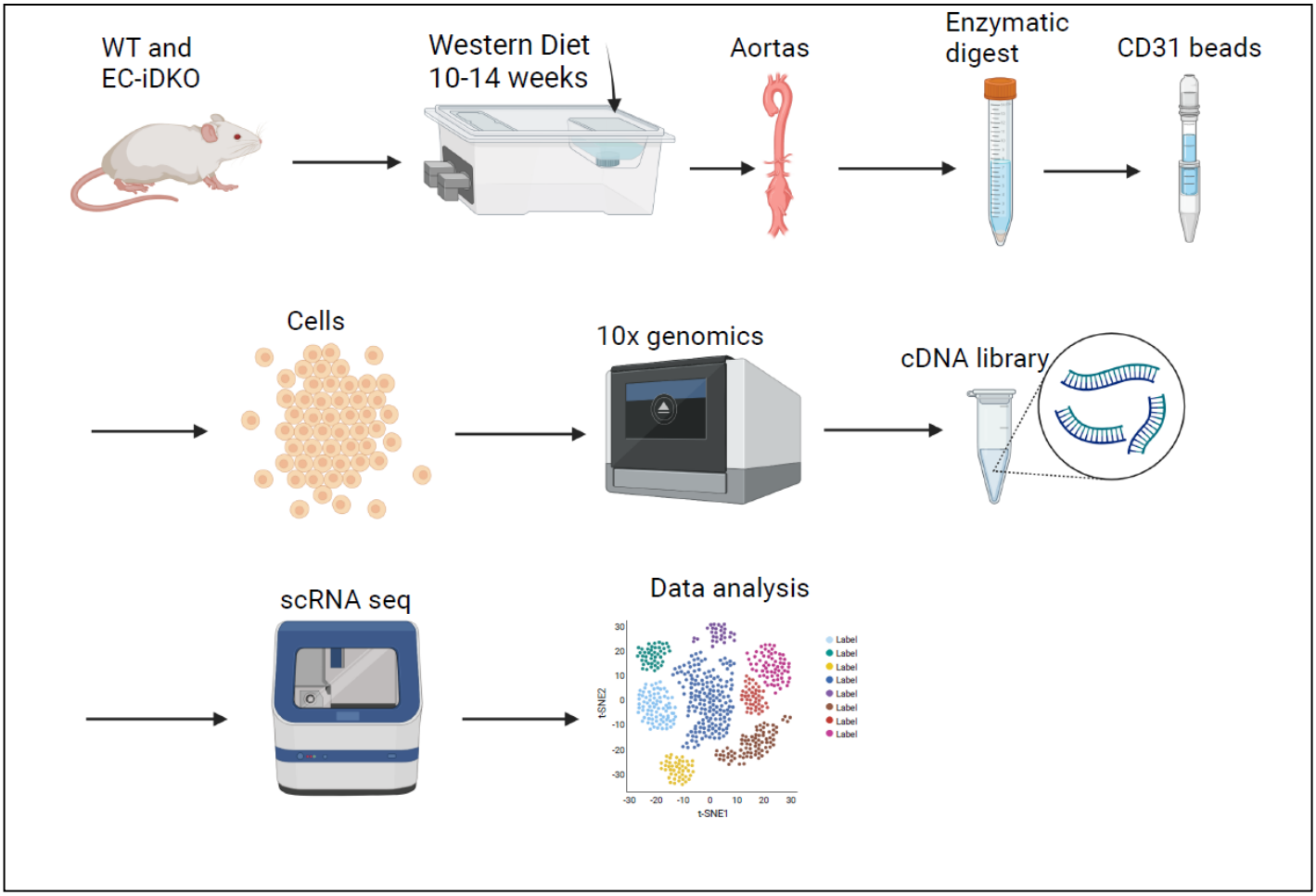

Supplemental Figure 2. Procedure for single cell RNA sequencing (scRNA seq).
WT and EC-iDKO mice were fed WD as indicated time, followed by the isolation of aortas, enzyme digestion and pass through CD31 beads to enrich endothelial cells, and the barcoding cells in 10 x genomics as company instruction. cDNA library was constructed and then perform scRNA seq and data analysis.

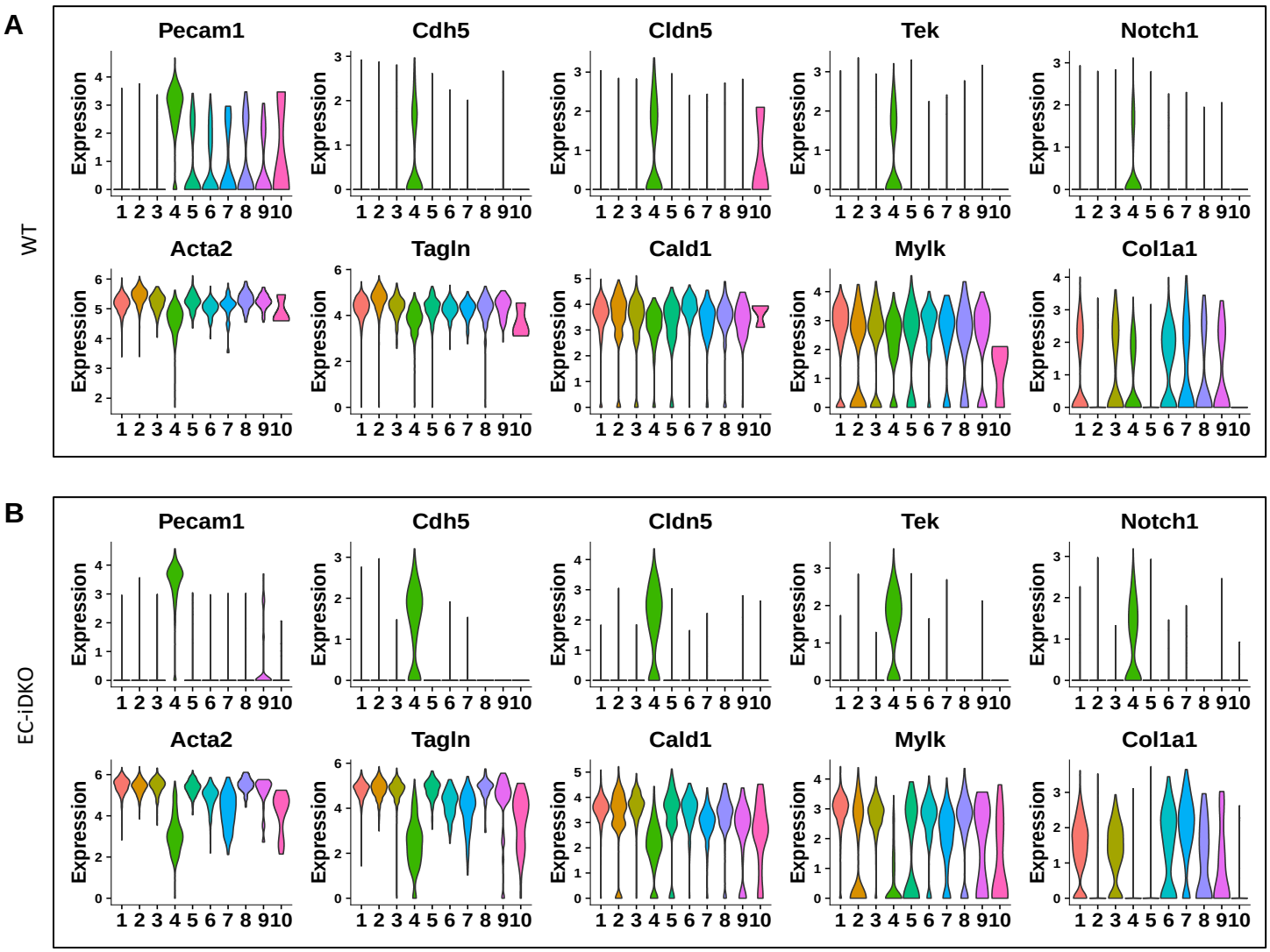

Supplemental Figure 3. Clustering annotation for single cell transcriptome in EndoMT models.
Violin plot of EC and SMC markers in EC-iDKO and WT cells. EC markers: Pecam1, Cdh5, Cldn5, Tek and Notch1; SMC markers: Acta2, Tagln, Cald1, Mylk and Col1a1.
(**A**) WT; (**B**) EC-iDKO

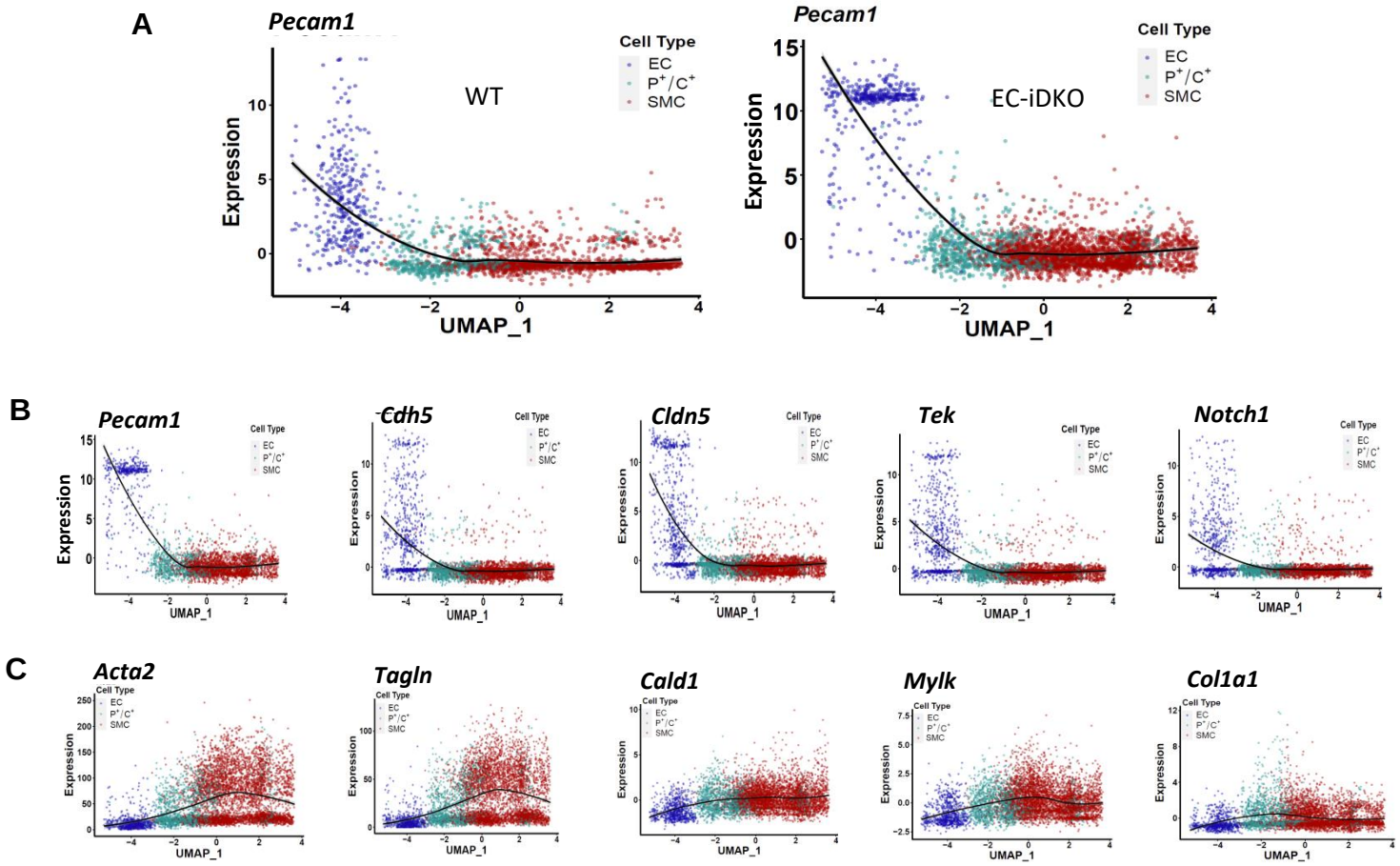

Supplemental Figure 4. Trajectory plots suggest EndoMT in the integrated cell population. (**A**) Pecam1 plot in EC-iDKO and WT cell population; (**B**, **C**) Trajectory Plot of EC markers and SMC markers in integrated cell population.

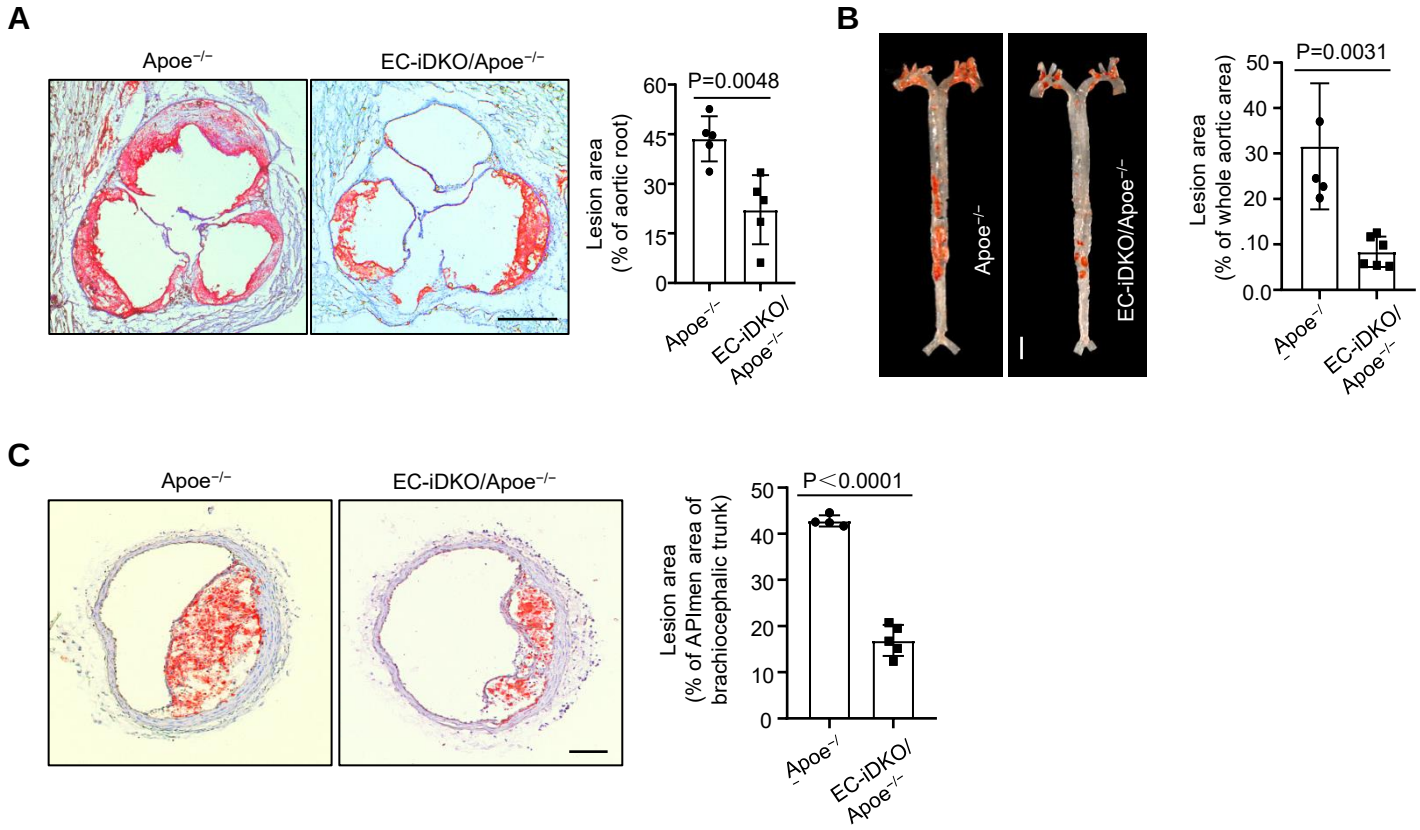

Supplemental Figure 5. Loss of endothelial epsins reduces atherosclerosis in Apoe$^{-/-}$ atherosclerotic models.

(**A**, **B**) ORO staining for aortic roots (**A**) and arch (**B**) of Apoe$^{-/-}$ and EC-iDKO/Apoe$^{-/-}$ mice fed WD for 12 weeks. n=5 in each group, p=0.0031. Scale bar: 500 μm (**A**); 5 mm (**B**).

(**C**) ORO staining for BCA from the mice as above, n=5 in each group, P<0.0001. Scale bar: 200 μm.

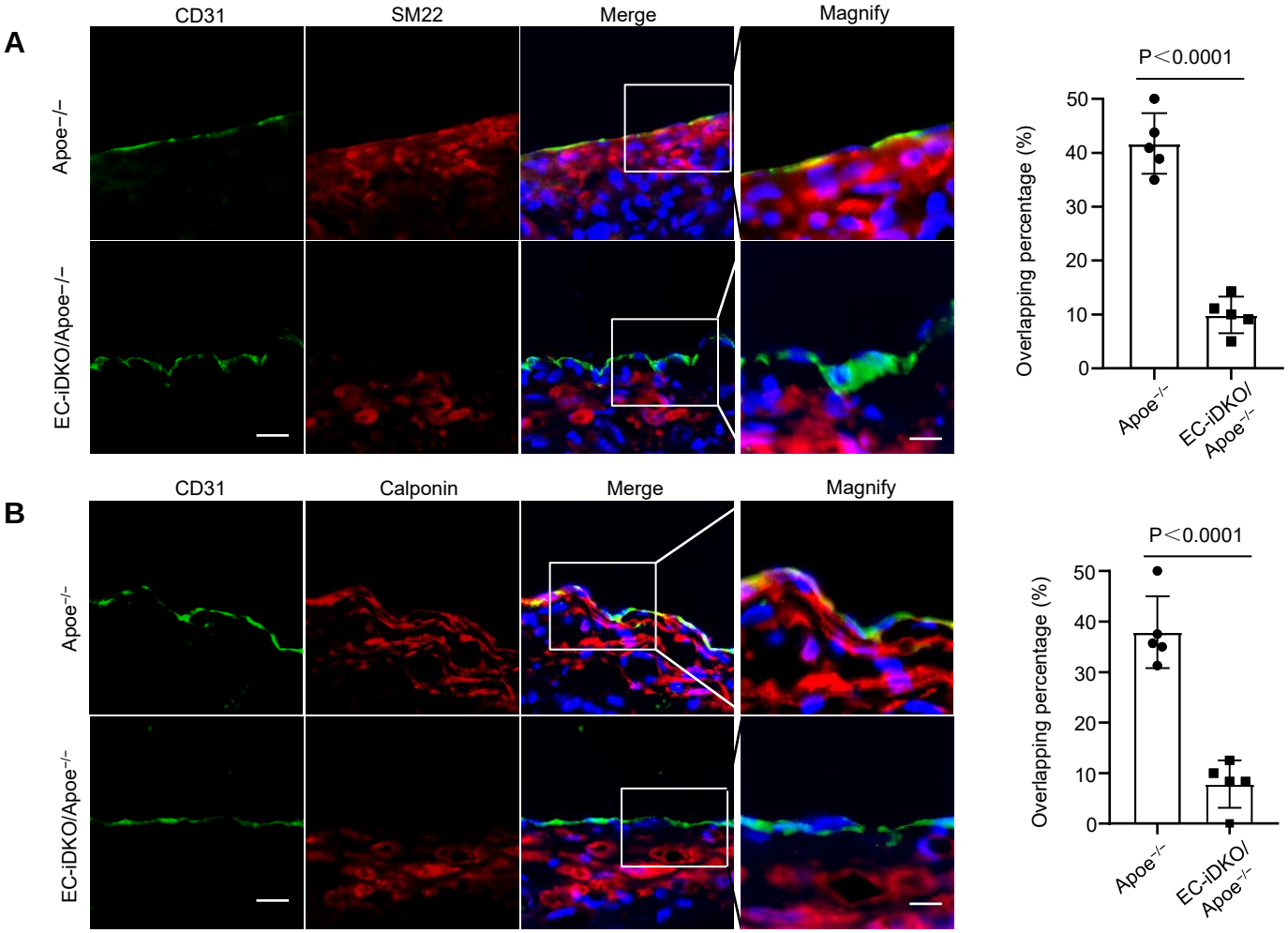

Supplemental Figure 6. Loss of endothelial epsins inhibits EndoMT in aortic root.
Apoe$^{-/-}$ or Epsin1f/f: Epsin 2$^{-/-}$: iCDH5-cre was injected tamoxifen to delete Epsin1 in vivo, and mice were fed WD for 12 weeks.
(**A**) CD31 and SM22 co-staining. n=5 mice in each group, P<0.0001.
(**B**) CD31 and Calponin co-staining. n=5 mice in each group, P<0.0001.
Scale bars: E& F, 20 μm, Magnified, 10 μm.

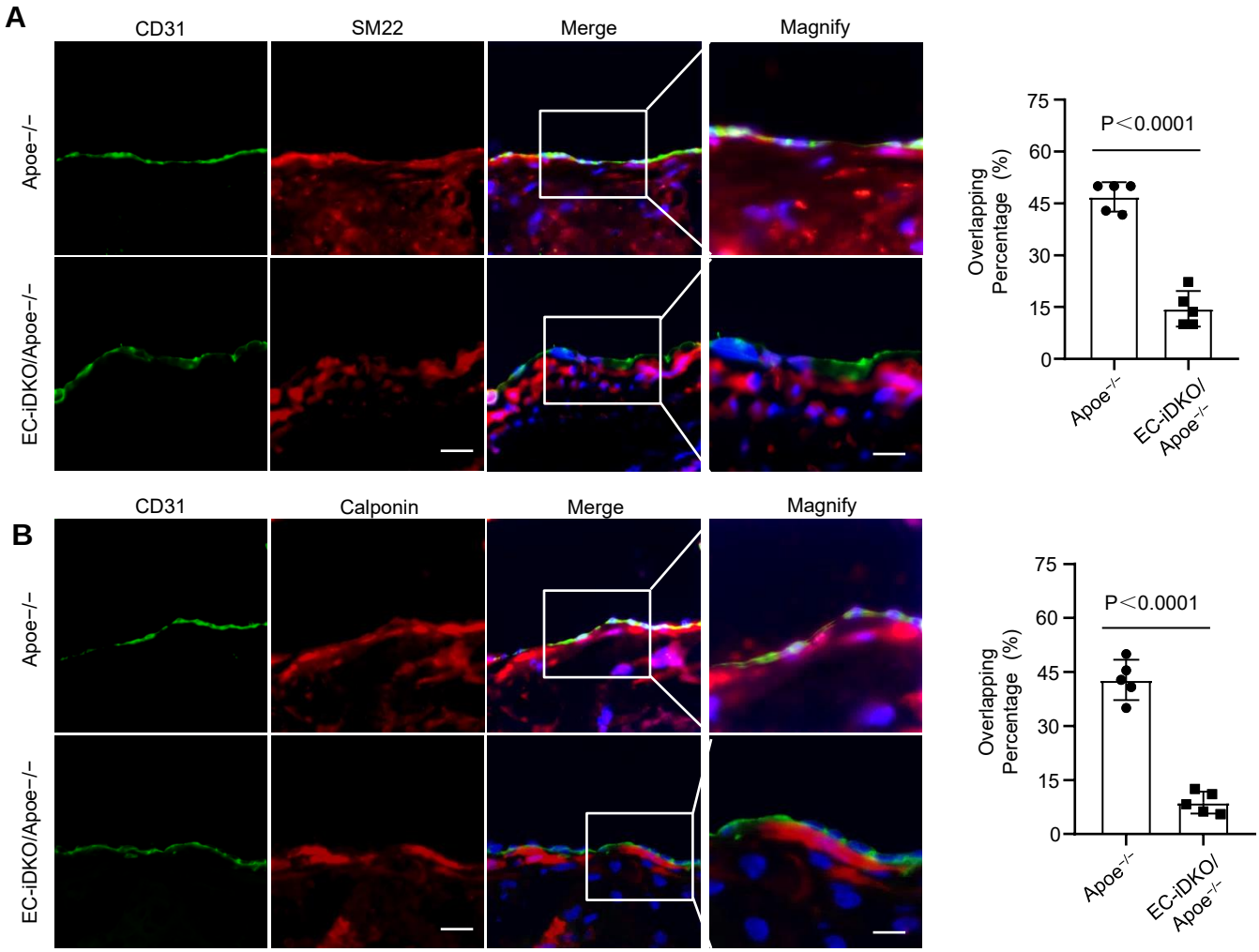

Supplemental Figure 7. Loss of endothelial Epsins inhibits End MT markers in the BCA region of aortas of Apoe$^{-/-}$ atherosclerotic model.

(**A**) CD31 and SM 22 co-staining. n=5 mice in each group, P<0.0001.

(**B**) CD31 and Calponin co-staining. n=5 mice in each group, P<0.0001.

Scale bars: A& B, 20 μm, Magnified, 10 μm.

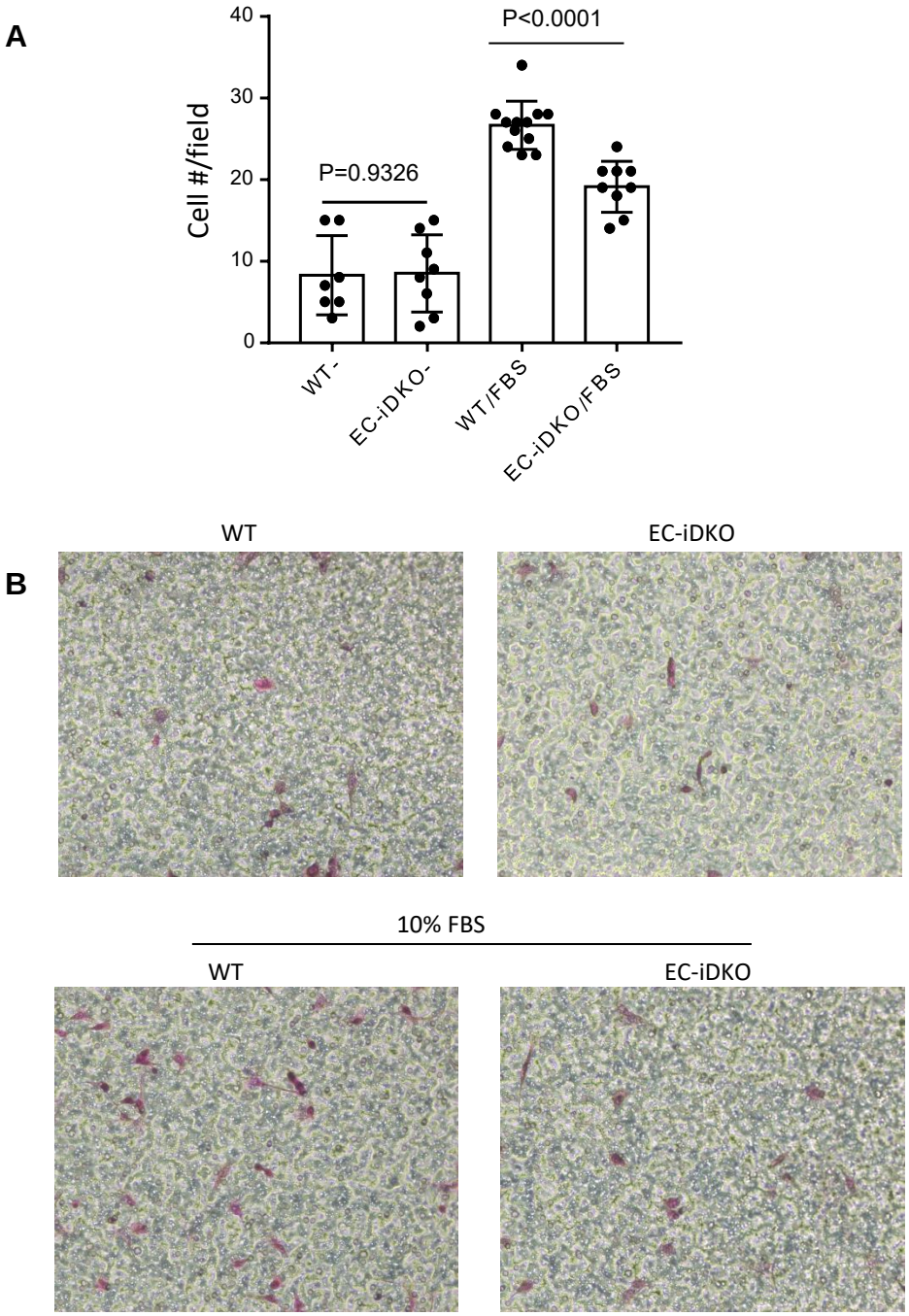

Supplemental Figure 8. Migration assay of MAECs of WT and iDKO treated by TGFβ1.
MAEC cells treated by 10 ng/ml TGFβ for 7 days, followed by Transwell migration assay (7 hours).
(A) Statistical result from Transwell Migration Assay; n=5 field in three independent experiments;
(B) Representative images of WT and EC-iDKO cells treated by TGFβ and migration assay after 7 hours in Transwell.

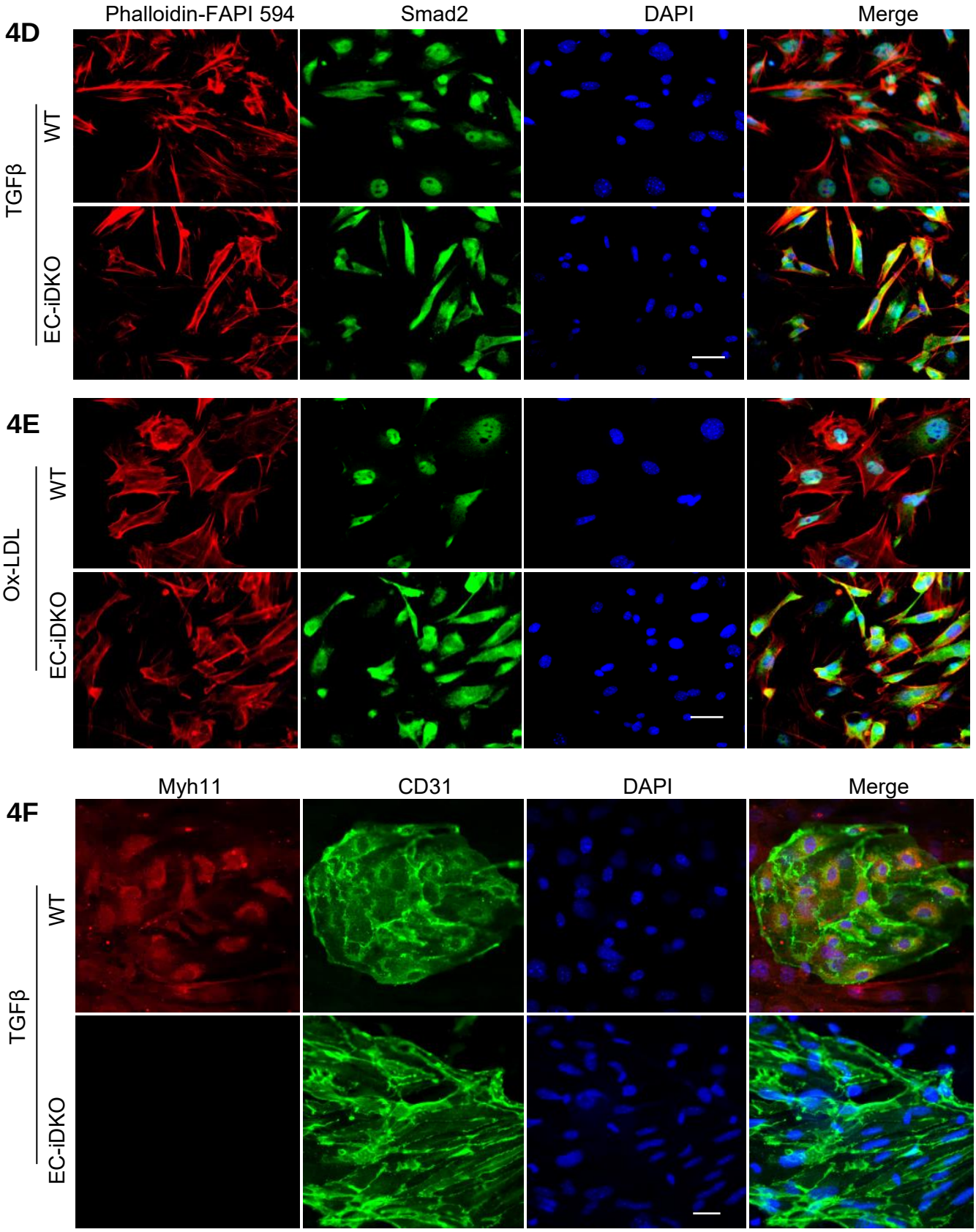

Supplemental Figure 9. Close-up view (individual panels) of Figure 4D, 4E and 4F.
4D, 4E, Smad2 translocation was measured by immunofluorescent co-immunostaining Smad2 and Phalloidin-Flu 594. MAECs of WT and EC-iDKO were treated by 10 ng/ml TGFβ or 100 μg/ml oxLDL for 5 days. n=5, P<0.001.
4F, Co-immunostaining of CD31 and Myh11 for MAECs of WT and EC-iDKO treated by 10 ng/ml TGFβ for a week. n=7, P<0.001. Scale bars: 50 μm for (D, E, F). Magnified in (F): 25 μm

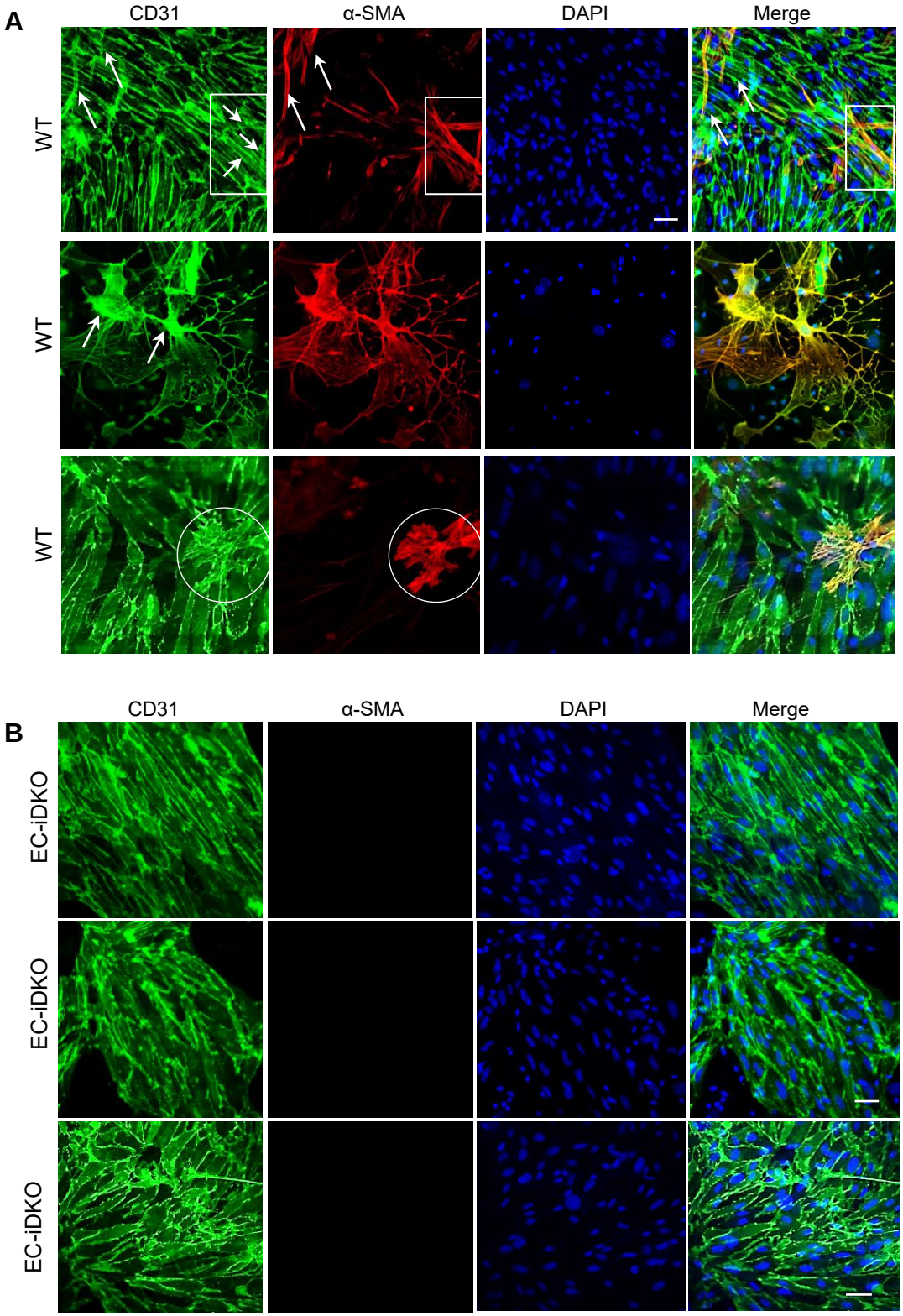

Supplemental Figure 10. Loss of epsins in endothelium attenuates EndoMT markers promoted by TGFß treatment in vitro, showing more representative EndoMT examples in WT MAECs.
MAECs isolated from WT or EC-iDKO mice and treated by TGFβ (10 ng/ml) for 15 days. TGFβ will be replaced every-other-day. During the treatment time, tamoxifen will be always supplied in the medium at 1 μM for both WT and EC-iDKO cells. Circle: SMC-like cells; Arrows: EC is becoming SMC-like cells induced by TGFβ. Scale bar: 25 μm.

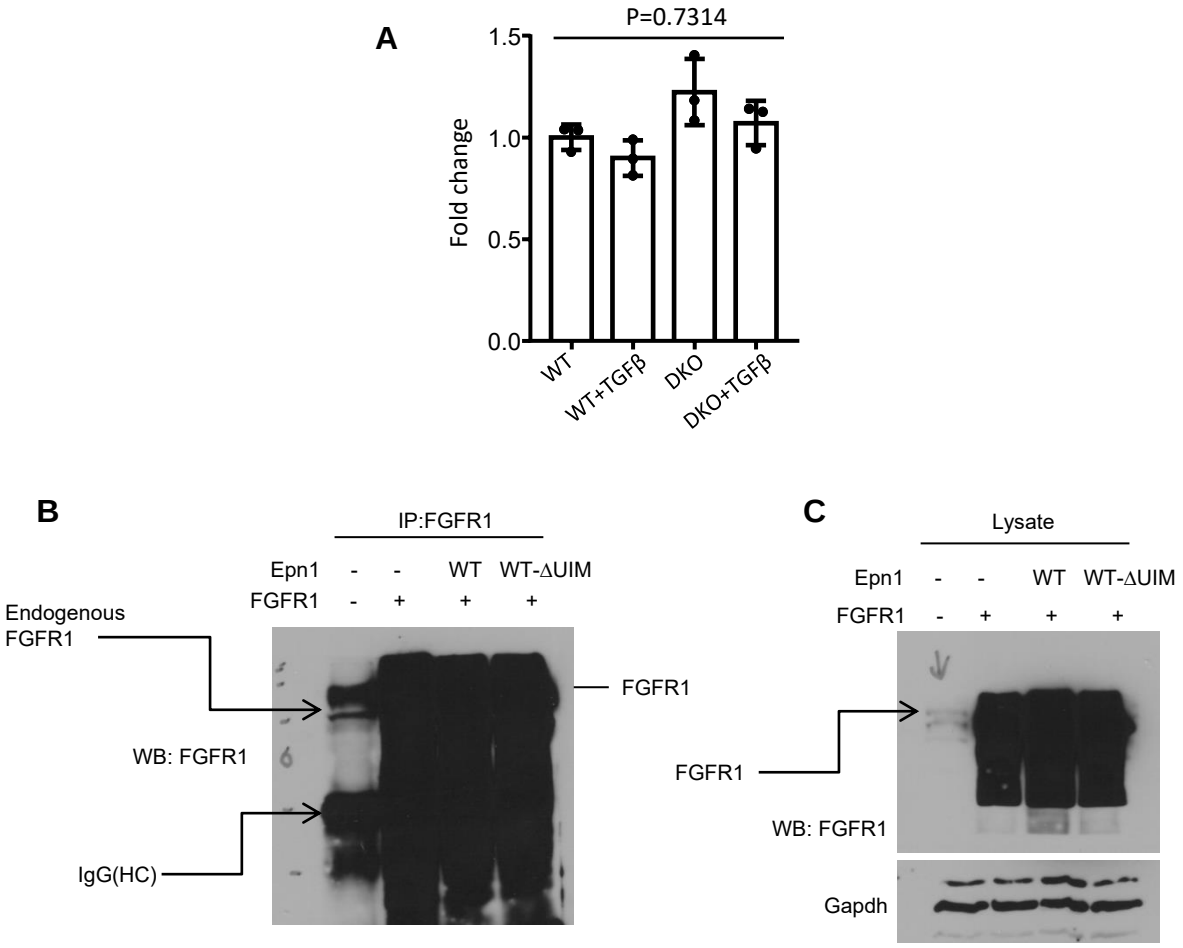

Supplemental Figure 11. **mRNA expression of FGFR1 in MAECs of WT and DKO and Longer time exposure of western blot in main Figure 4K and 4M.**

(**A**) qPCR test for FGFR1 transcriptional expression in MAECs of WT and DKO cells with or without TGFβ (10 ng/mL) treatment for 24 hours;

(**B**, **C**) Longer time exposure of western blot in main Figure 4K and 4M, i.e. IP and input samples, showing endogenous FGFR1 bands in IP (Fig. 4K) or cell lysate (Fig. 4M) separately.

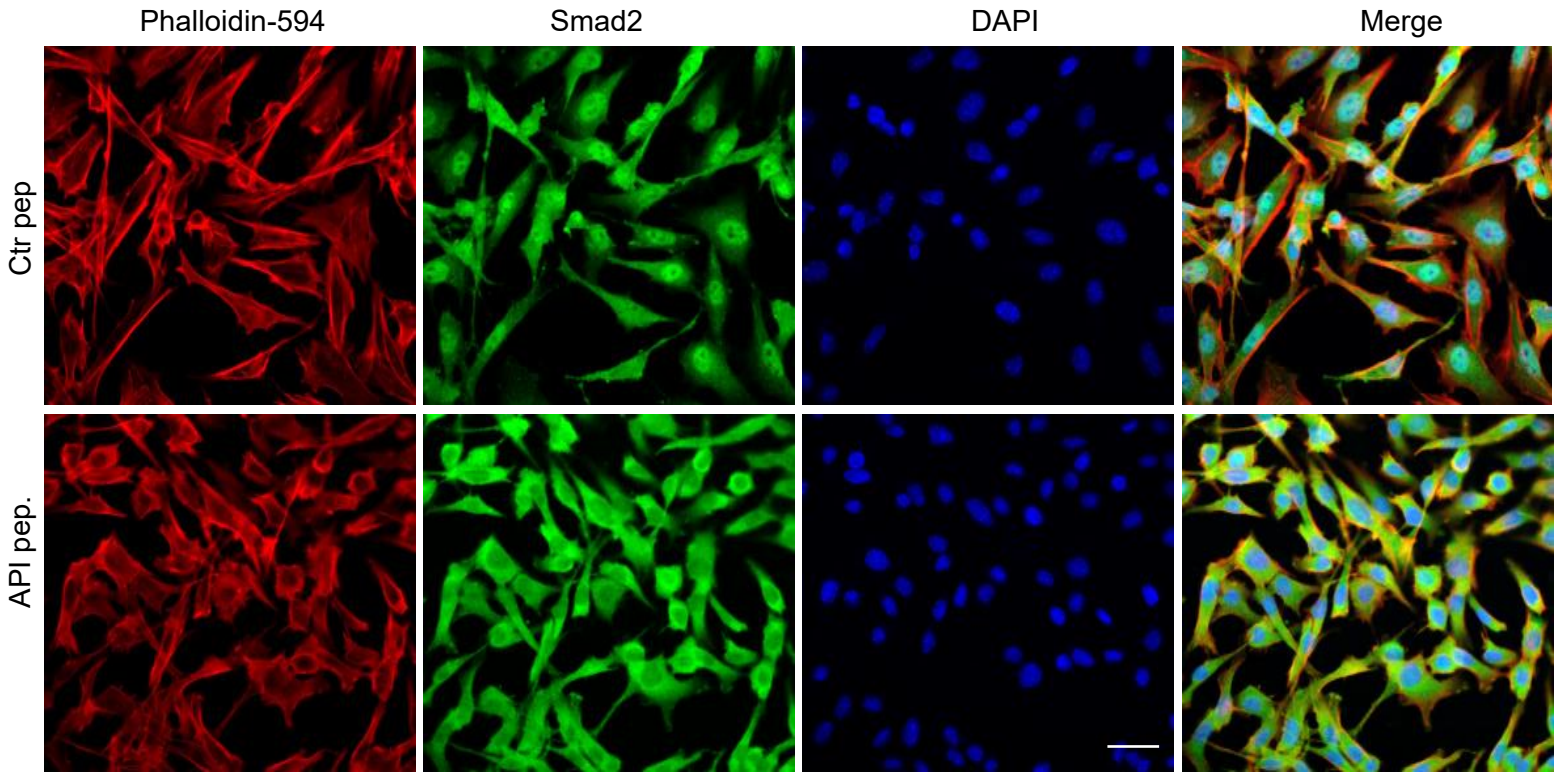

Supplemental Figure 12. Close-up view (enlarged view) of Figure 6F

Showing Smad2 nuclei staining in Ctr peptide, and API peptide inhibits nuclei translocation. WT MAECs were pre-loaded with 50 μM control or API peptide, followed by the treatment of TGFβ (10 ng/ml) for 3 days, and co-stained Smad2 nuclei translocation with Phalloidin-594; n=8, *P<0.001. Scale bar: 20 μm.

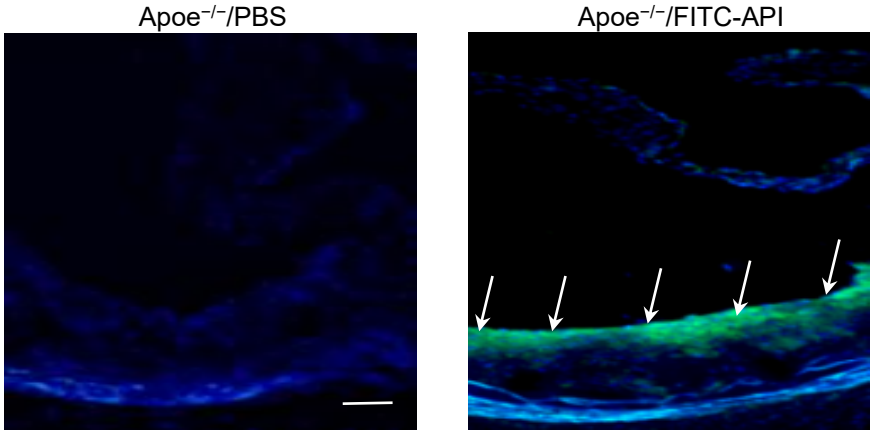

Supplemental Figure 13. FITC-conjugated API peptide (50 mg/kg, i.v injection) can be targeted to atheroma region in *Apoe*$^{-/-}$ mouse model fed WD for 6 weeks.
Green color is the FITC concentrated area (FTIC-API). Scale bar: 500 μm.

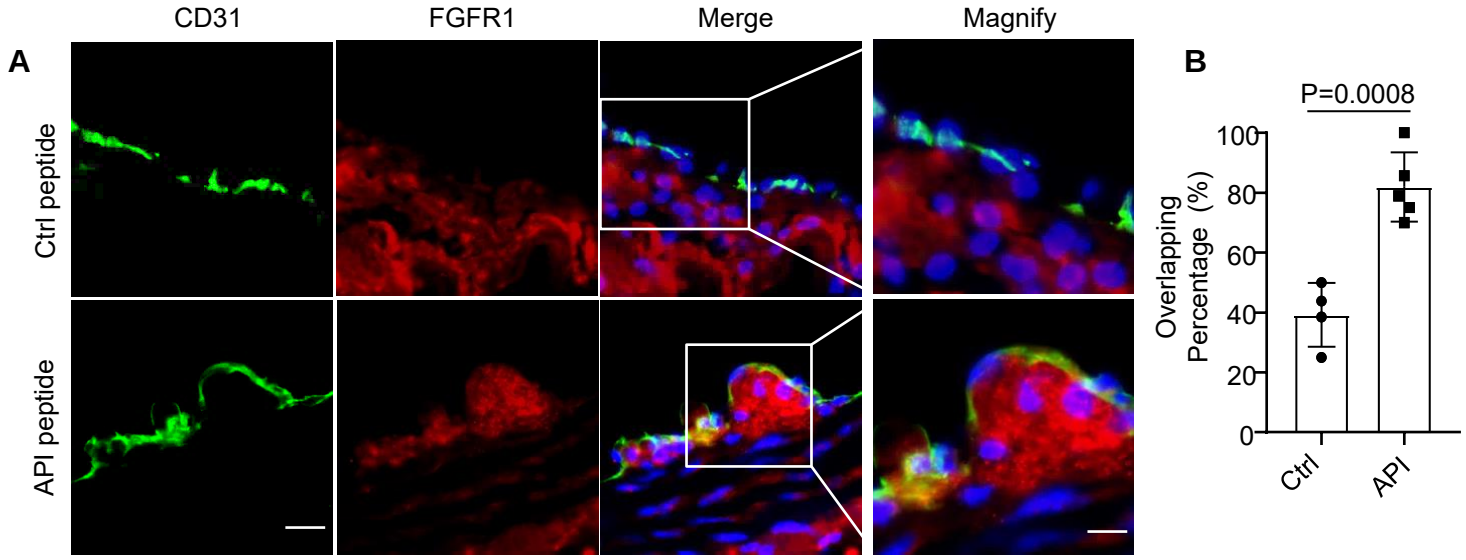

Supplemental Figure 14. API peptide administration increasing FGFR1 expression in *Apoe*$^{-/-}$ mouse model. *Apoe*$^{-/-}$ mouse models were administrated with Ctr peptide or API peptide for 12 weeks (50mg/kg, I.V.), BCA was selected for FGFR1 immunofluorescent staining. n=5, P=0.0008, Ctr peptide *vs* API peptide. Scale bar: 20 μm, and magnified: 10 μm.

Mouse genes	Primers (5'-------→3')
Claudin-5 (CLDN5)	ClDN5_L1 5-TCTGGTGCTGTGTCTGGTAG ClDN5-R1 5-GTCACGATGTTGTGGTCCAG
VE-Cadherin	VE-Cadherin_L1 5- TACCACTTCAAGCTGCCAGA VE-Cadherin_R1 5-TCGGAAGAATTGGCCTCTGT
PECAM-1 (CD31)	PECAM-1_L1 5-GGTCGTGAATGACACCCAAG PECAM-1_R1 5-ACTCTGACTGCAAGAGTGCT
vWF	vWF_L1 5-GCCAGTATGTTCTGGTGCAG vWF_R1 5-CGTTCACCTCTCCGTCAAAC
Acta2 (α-SMA)	Acta2_L1 5-GTCCCTCTATGCCTCTGGAC Acta2_R1 5-AAGGAATAGCCACGCTCAGT
MMP2	MMP2_L1 5-GACAGGTGACCTTGACCAGA MMP2_R1 5-TAGTTGGCCACATCTGGGTT
Snail1	Snail1_L1 5-CCCACTCGGATGTGAAGAGA Snail1_R1 5-AGACTCTTGGTGCTTGTGGA
Slug	SAPIg_L1 5-ACTACAGCGAACTGGACACA SAPIg_R1 5-GCCACTGGGTAAAGGAGAGT
Twist1	Twist1_L1 5-GACTCCAAGATGGCAAGCTG Twist1_R1 5-CCATCCTCCAGACGGAGAAG
Fibronectin (Fn1)	Fibronectin_L1 5-TCACCTACGGAGAGACAGGA Fibronectin_R1 5-TGTTGTTGATGGTGGCTGTG
Collagen 1a (Col1a1)	Collagen 1_L1 5-AGGGTGACAAAGGAGAGGTG Collagen 1_R1 5-AGGTGGAAGAGGTCAATGGG
Vimentin (VIM)	Vimentin_L1 5-AAGACTCGGTGGACTTCTCG Vimentin_R1 5-TCGATGTAGTTGGCAAAGCG
N-Cadherin	N-cadherin_L1 5-GAAGGATGTGCACGAAGGAC N-cadherin_R1 5-AGGGAAGCTTCTCACAGCAT
FAP	FAP_L1 5-ATAGCAGTGGCTCCAGTCTC FAP_R1 5-TCATCTGCTGTTCCGTGGAT
FSP1 (S100A4)	FSP1_L1 5-AGCTGCATTCCAGAAGGTGA FSP1_R1 5-ATGCAGGACAGGAAGACACA
TGFbR1	TGFbR1_L1 5-TGTCATTGCTGGTCCAGTCT TGFbR1_R1 5-CTCTTCATTTGGCACACGGT
FGFR1	FGFR1_L1 5-TGATGACGACGACGATGACT FGFR1_R1 5-TACAGGCCTACGGTTTGGTT

Supplemental Table S1: Primers used in the RT-PCR for mouse EndoMT marker genes

Antibody	Sources	Cat#	Source/ Isotype	Applications	Cross activity	MW (kDa)
FGFR1	Cell signaling	9740	Rabbit IgG	WB, IP, IF, IHC, F	H M R Mk	92 , 120, 145
Smad2	Cell signaling	5339	Rabbit IgG	WB, IP, IF, CHIP, F	H M R Mk	60
P-Smad2	Cell signaling	3108	Rabbit IgG	WB	H M R Mi	60
Smad5	Cell signaling	12534	Rabbit IgG	WB, IP, CHIP	H M R Mk	60
P-Smad1/5	Cell signaling	9516	Rabbit	WB, IF, F	H M R	60
Phalloidin-594	Abcam	ab176757	MS	IF (red)	M H	
Snail	Cell signaling	9585	Rabbit IgG	WB, IP, IF, F	H M	30
N-Cadherin	Cell signaling	4061	Rabbit	WB	H M R Mk	140
Vimentin	Dako	M7020	MS	IF	H M	
α-SMA-cy3	Sigma	C6198-.2ml	MS	IF	H M	
VE-Cadherin	Santa Cruz	Sc-9989	MS	IF	M H	
MYH11	Abcam	ab224804	Rabbit	IF, WB	M R H	42
SM22 (Tagln)	Abcam	ab14106	Rabbit	IF, WB	M R H	23
Calponin	Abcam	ab46794	Rabbit	IF	M R H	
CD31	BD Pharmingen	550274	Rat	IF	M H R	
CD68	Santa Cruz	Sc-20060	MS	IF	M H	
Epsin 1	Home made	n/a	Rabbit	WB, IP, IF	H M	75~80
Epsin 2	Home made	n/a	Rabbit	WB, IP, IF	H M	65~70
HA.11	BioLegend	901502	MS	WB, IP	all	n/a
Flag	Cell signaling	14793	Rabbit IgG	WB,IP,IHC,IF,F,ChIP	all	n/a
α-Tubulin-c	DSHB	12G10	MS	WB	M R, etc	50
ß-actin	Cell signaling	4967	Rabbit	WB	H M R, etc	45
GAPDH	Santa Cruz	Sc-166545	MS	WB	H M	37-43

Secondary antibodies used in our laboratory (Products of Invitrogen)

Alexa Fluor 488 (Green)	Alexa Fluor 594 (Red)	Alexa Fluor 647 (Blue)
Donkey anti-Mouse (A21202)	Donkey anti-Mouse (A23744)	Donkey anti-Mouse (A31571)
Donkey anti-Rabbit (A21206)	Donkey anti-Rabbit (A21207)	Donkey anti-Rabbit (A31573)
Donkey anti-Rat (A21208)	Donkey anti-Rat (A21209)	Goat anti-Rat (A21247)
Donkey anti-Goat (A11055)	Donkey anti-Goat (A11058)	

Supplemental Table S2: Source of antibodies used in this study